IIETA International Information and Engineering Technology Association
Advancing the World of Information and Engineering

Mathematical Modelling of Engineering Problems
Vol. 13, No. 4, April, 2026, pp. 663-683
Journal homepage: http://iieta.org/journals/mmep

Hybrid Meta-Heuristic Optimization Algorithms with Integral Sliding Mode Control: Applied to Control Permanent Magnet Synchronous Generator-Based Wind Energy System

Marwa Arabi[1], Youcef Zennir[1], Hicham Bounezour[1], Mohamed Benghanem[2*]

[1] Automatic Laboratory of Skikda, University of 20 August 1955 - Skikda, Skikda 21000, Algeria
[2] Physics Department, Faculty of Science, Islamic University of Madinah, Madinah 42351, Saudi Arabia

Corresponding Author Email: mbenghanem@iu.edu.sa

https://doi.org/10.18280/mmep.130405

Received: 14 October 2025
Revised: 7 December 2025
Accepted: 15 December 2025
Available online: 15 May 2026

Keywords:
Permanent Magnet Synchronous Generator, Field-Oriented Control, Integral Sliding Mode Control, optimization, Particle Swarm Optimization, Particle Swarm Optimization-fmincon, Grey Wolf Optimizer

ABSTRACT

This study presents a comparative analysis of the performance of standard metaheuristic algorithms and their hybrid variants for tuning the parameters of an Integral Sliding Mode Controller (ISMC) applied to a Permanent Magnet Synchronous Generator (PMSG) in wind energy conversion systems. Specifically, the Particle Swarm Optimization (PSO) and Grey Wolf Optimizer (GWO) are investigated, along with two hybrid strategies: PSO combined with the MATLAB-based nonlinear constrained solver *fmincon*, and a PSO–GWO hybrid approach. These optimization techniques are employed to improve the dynamic performance and robustness of the ISMC under varying wind conditions. The optimized controllers are benchmarked against the conventional Integral Sliding Mode–Field-Oriented Control (ISM–FOC) scheme. All simulations are conducted in the MATLAB/Simulink environment. Results show that the conventionally tuned ISMC exhibits a slower response and higher current-tracking errors, with the quadrature current error reaching approximately 0.2 and the direct current oscillating around 5×10^{-6} A, with a response time of 4.5×10^{-3} s. The results clearly demonstrate that the proposed optimization approaches significantly enhance control accuracy, reduce tracking errors, and mitigate chattering effects.

1. INTRODUCTION

Faced with a continuously rising global demand for electricity that driven by rapid urbanization, industrial expansion, transportation electrification, and the proliferation of data centers, the need for sustainable and low-carbon energy production has become an urgent global priority [1]. In 2024, global electricity consumption increased by a record 4.3%, representing approximately 1,100 Terawatt-hour (TWh) of additional demand—nearly double the average annual growth rate of the past decade [2]. This surge is mainly attributed to the rise in electric vehicle adoption, increased use of air conditioning due to extreme temperatures, and the escalating energy requirements of data centers powering artificial intelligence applications [3].

Simultaneously, renewable energy sources have played a pivotal role in meeting this rising demand. In 2024, global installed wind energy capacity reached 1,174 Gigawatt (GW), with 121 GW added in that year alone, accounting for approximately 11% of global electricity generation [4]. This rapid expansion underscores the growing significance of wind energy within the global energy mix.

Wind Energy Conversion Systems (WECS) are central to this energy transition. A typical WECS consists of a wind turbine that transforms the kinetic energy of wind into mechanical energy, which is then converted into electrical energy by a generator. These systems are generally classified into two main types: fixed-speed and variable-speed turbines. Fixed-speed (often employing squirrel cage induction generators) are known for their simplicity and robustness, but offer limited efficiency under varying wind conditions. Conversely, variable-speed systems dynamically adjust their rotor speed in response to wind fluctuations, thereby maximizing energy capture. These systems typically utilize either Doubly-Fed Induction Generators (DFIGs) or Permanent Magnet Synchronous Generators (PMSGs) [5-7].

Among these, PMSG-based WECS have attracted considerable attention due to their high efficiency, compactness, absence of brushes and slip rings, and reduced maintenance requirements [5, 6]. However, WECS are inherently nonlinear systems subject to significant uncertainties and disturbances, primarily due to the stochastic nature of wind speeds [6, 8]. These challenges emphasize the need for robust control strategies to ensure reliable and efficient operation, particularly under variable environmental conditions [7-9].

To address these challenges, extensive research efforts have focused on enhancing the control performance of WECS. Field-Oriented Control (FOC), applied primarily to the Machine-Side Converter (MSC) in PMSG-based systems, has emerged as one of the most widely adopted techniques due to its capability to decouple torque and flux control [9, 10]. Nevertheless, traditional FOC methods are highly sensitive to parameter variations, model uncertainties, and external

disturbances, which can degrade system performance under turbulent wind scenarios [10, 11].

To overcome these limitations, several advanced control strategies have been proposed. Recent control approaches for PMSG-based WECSs have increasingly focused on enhancing robustness and mitigating chattering effects, while simultaneously introducing greater computational complexity and tuning challenges. Majout et al. [12] proposed a smooth switching sliding mode control (SMC) that improves speed tracking accuracy and system stability while reducing current ripple; this contribution highlights the potential of continuous switching surfaces to limit the discontinuities inherent to classical SMC, yet the drawback lies in the fact that the smoother transitions inevitably introduce dynamic latency and make the controller more difficult to implement in practice due to added design complexity. Zine Laabidine et al. [13] developed an adaptive super-twisting sliding mode control (AST-SMC) that nearly eliminates chattering through online gain adjustment, thereby improving robustness under parameter variations and disturbances. Nevertheless, this technique remains heavily dependent on high-precision sensors and mathematically demanding gain adaptation laws, which may complicate real-time application. More recently, Douara et al. [14] combined a second-order terminal attractor (SO-STA) with a super-twisting algorithm (STA) in a high-order hybrid structure to benefit from fast convergence and enhanced robustness, where the synergy between finite-time convergence and continuous control law reduces steady-state error; however, the intricate tuning procedure still represents a barrier for practical deployment. In parallel, Belabbes et al. [15] integrated a model predictive control (MPC) strategy with conventional SMC to reduce harmonic distortion and tracking error, demonstrating how predictive horizons can improve dynamic performance and minimize oscillations. Yet, this hybridization requires powerful computational platforms and advanced solvers, making the solution less attractive for cost-sensitive applications. Earlier works by Messadi et al. [16] and Aboulem et al. [17] explored MPC for stabilizing chaotic dynamics and PSO-optimized PI-SMC controllers to reinforce robustness, although neither approach fully eliminates chattering nor resolves practical implementation challenges.

SMC has emerged as a powerful nonlinear control method, enforcing system trajectories to converge toward a predefined sliding surface, thereby ensuring fast response and robustness against matched uncertainties [18]. However, conventional SMC suffers from chattering phenomena and may induce steady-state errors if boundary layer conditions are not properly tuned. The Integral Sliding Mode Control (ISMC) approach mitigates these issues by introducing an integral action into the sliding surface, eliminating the reaching phase and significantly reducing chattering. By enforcing the system trajectory to lie on the sliding manifold from the initial time, ISMC enhances robustness and ensures smoother control action. Yet, in practice, selecting appropriate values for the integral gain and sliding coefficients remains a nontrivial challenge, as improper tuning may deteriorate both dynamic response and steady-state accuracy, thus negating the theoretical benefits of ISMC [18].

In order to overcome these limitations, our contribution relies on metaheuristic optimization algorithms for the automatic tuning of ISMC parameters. This approach significantly reduces model dependency, since the controller gains are directly adjusted based on performance criteria, thereby enhancing robustness against uncertainties and parameter variations. It also preserves the structural simplicity of the control law by avoiding the introduction of additional layers of complexity (fuzzy, adaptive, or high-order), which facilitates practical implementation. Moreover, optimization improves dynamic performance by simultaneously minimizing tracking error, response time, and oscillation amplitude, thus ensuring an optimal trade-off between robustness and speed. The method further offers high flexibility, as it can be adapted to various environments and system types (linear, nonlinear, or disturbed) depending on the chosen algorithm (PSO, Genetic Algorithms, GWO, or hybrid approaches). Finally, unlike certain ISMC variants requiring complex online adaptation, our method enables offline computation of optimal parameters, thereby significantly reducing the computational burden during controller execution. The originality of our work therefore lies in combining the inherent robustness of ISMC with the exploration capability of metaheuristic algorithms, while overcoming the main drawbacks of existing methods, such as excessive complexity, high computational cost, and strong model dependency. To address the challenging task of ISMC tuning, advanced methods such as Particle Swarm Optimization (PSO) and Grey Wolf Optimizer (GWO) are employed. PSO is frequently chosen for its intuitive implementation and powerful global-search capability. It operates by simulating the collective behavior of swarms, which allows for efficient exploration of the search space. However, when applied to high-dimensional or multi-objective problems, PSO may exhibit premature convergence or slow adaptation to rapidly changing dynamics, limiting its reliability in real-time wind energy applications [19-21]. A recent study [22] has applied PSO to parameter estimation in a chaotic system and discussing PSO dynamics.

The GWO, which mimics the leadership hierarchy and cooperative-hunting strategies of grey wolves, balances exploration and exploitation more adeptly through its encircling and hunting mechanisms. Despite this advantage, GWO can still face premature convergence and shows strong sensitivity to its internal coefficients, making its effectiveness dependent on careful parameter calibration [23]. Hybridizing these metaheuristics has emerged as a particularly effective remedy. By coupling PSO's swarm-based exploration with MATLAB's gradient-driven *fmincon* solver, the PSO-*fmincon* variant capitalizes on both broad search and precise local refinement. Likewise, embedding GWO's pack-hunting dynamics into the PSO framework (GWO–PSO) endows the swarm with additional mechanisms to evade local traps and accelerate convergence toward the global optimum [24].

The primary objective of this study is to enhance the performance of the ISMC for a PMSG-based WECS by employing metaheuristic optimization schemes that automatically determine its gains according to explicit performance criteria. Rather than modifying the ISMC structure itself, the proposed approach demonstrates that an optimally tuned classical ISMC can achieve high robustness, effective chattering mitigation, low computational burden, and straightforward implementation.

The originality of this work lies in the application of different metaheuristique optimization algorithms for the optimization of ISMC parameters in a PMSG, given that none of the previously used metaheuristics had been exploited for tuning this simple yet robust control law.

Building upon this framework, the present study conducts a rigorous comparative evaluation of four optimization

algorithms standard PSO, standard GWO, PSO-*fmincon*, and the hybrid GWO–PSO for automatic ISMC gain tuning within the field-oriented control loop of a PMSG-based wind turbine. The assessment focuses on convergence speed, robustness to parameter uncertainties, chattering suppression, and overall energy-capture efficiency under realistic variable-wind scenarios, thereby identifying the most effective optimization strategy for enhancing ISMC-controlled PMSG performance.

The insights gained will guide the design of more reliable and high-performance control systems for next-generation wind-energy converters. The structure of the rest paper is organized as follows: Section 2 presents the mathematical modeling of the main components of the WECS. Subsequently, Section 3 introduces the fundamental control strategies employed, namely FOC, SMC, and its enhanced version, ISMC. Then, Section 4 details the optimization algorithms and the hybridization techniques implemented to improve the tuning of controller parameters. Following this, Section 5 outlines the implementation steps, the simulation setup, and provides a thorough comparative analysis of the obtained results. Finally, Section 6 concludes the paper and suggests directions for future research.

2. WIND ENERGY CONVERSION SYSTEM MODELING

2.1 Wind turbine modeling

The generation of a wind turbine involves an aerodynamic torque C_{aer} and mechanical power P_t, expressed as outlined in study [23]:

$$P_t = 0.5C_p(\lambda,\beta)\rho\pi R^2V^3 \text{ and } C_{aer} = \frac{P_t}{\Omega_t} \quad (1)$$

where, R is the dimension of the wind turbine rotor (m), V is the wind velocity (m/s), ρ is air density, and $C_p(\lambda,\beta)$ is the wind turbine power coefficient, which is then given as following:

$$C_p = \left[0.5176\left(\frac{116}{\lambda'}\right) - 0.4\beta - 5\right]exp\left(\frac{-21}{\lambda'}\right) + 0.0068\lambda \quad (2)$$

with

$$\lambda' = \frac{1}{\lambda + 0.08\beta} - \frac{0.035}{\beta^3 + 1} \quad (3)$$

$$\lambda = \frac{\Omega_{mec}R}{V} \quad (4)$$

where, λ is the tip-speed-ratio, Ω_t is the mechanical speed of the turbine blades (in rad/s), and β is the blade pitch angle.

The characteristics of the wind turbine [25] are shown in Figure 1.

Figure 1 presents the power coefficient (C_p) of the wind turbine as a function of the tip-speed ratio (TSR) for different pitch angles. At 0° pitch, the turbine reaches its maximum aerodynamic efficiency, showing the highest (C_p). As the pitch angle increases (2°, 5°, 10°, 15°, 20°), both the peak value of (C_p) and the optimal TSR decrease, indicating a progressive loss of efficiency. For high pitch angles, the extracted power becomes significantly reduced, reflecting the turbine's power-regulation behavior under high-wind conditions.

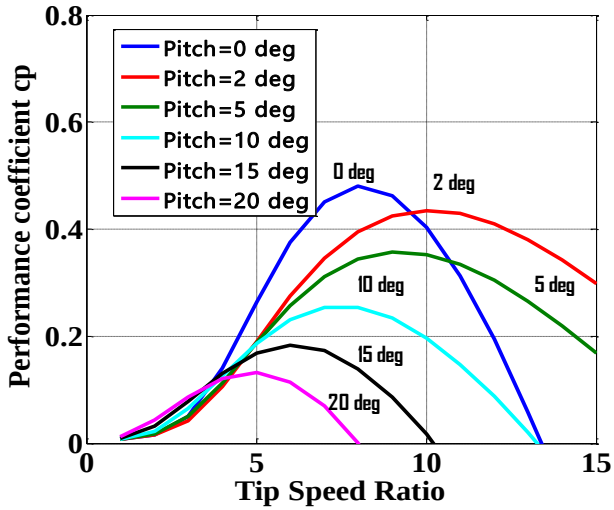

Figure 1. Aerodynamic power coefficient variation C_p against tip speed ratio λ and pitch angle β

As per Eq. (4), the mechanical torque of the wind turbine can be articulated as follows:

$$C_t = \frac{P_t}{\Omega_{mec}} = \frac{0.5C_p(\lambda,\beta)\rho\pi R^2V^3}{\Omega_{mec}} \quad (5)$$

The expressions related to the gearbox are showcased as follows:

$$C_t = \frac{\Omega_{mec}}{G} \quad (6)$$

$$\Omega_{mec} = G * \Omega_t \quad (7)$$

where, G is the gear ratio coefficient, Ω_{mec} is the mechanical rotational speed.

The illustration of the mechanical transmission is outlined as follows:

$$J\frac{d\Omega_g}{dt} = C_{mec} = C_g - C_{em} - C_f \quad (8)$$

Figure 2 visually presents the model [25] of the wind turbine.

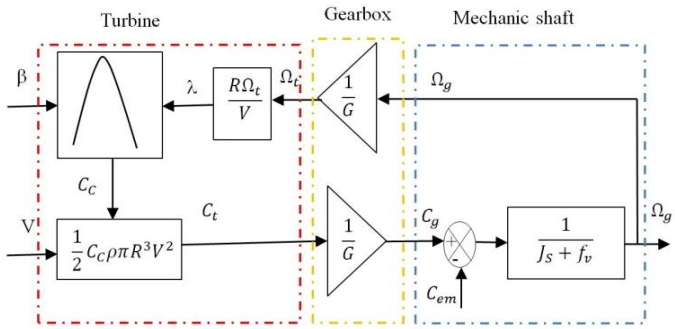

Figure 2. Horizontal axis wind turbine diagram block

2.2 Permanent Magnet Synchronous Generator

The generation of electromagnetic torque by the PMSG is depicted as shown below [18]:

$$C_{em} = \frac{3P}{2}(\lambda_r i_{qs} - (L_d - L_q) i_{ds} i_{qs}) \quad (9)$$

where, $L_d(H)$ and $L_q(H)$ are the dq-axis self-inductance of the synchronous generator, $\lambda_r(wb(rms))$ is the rotor flux linkages, P is the number of pole pairs, and i_{ds} and i_{qs} stand for the stator current along the dq-axis of the PMSG generator, as demonstrated in Eq. (10):

$$\begin{cases} \dfrac{di_{ds}}{dt} = -\dfrac{R_s}{L_d} i_{ds} + \dfrac{L_q}{L_d} w_r\, i_{qs} - \dfrac{1}{L_d} v_{ds} \\ \dfrac{di_{qs}}{dt} = -\dfrac{R_s}{L_q} i_{qs} + \dfrac{L_d}{L_q} w_r\, i_{ds} - \dfrac{1}{L_q} w_r\, \lambda_r - \dfrac{1}{L_q} v_{qs} \end{cases} \quad (10)$$

where, R_s represents the stator winding resistance of the PMSG generator, while v_{qs} and v_{ds} denote he dq-axis stator voltage:

$$\begin{cases} v_{ds} = -R_s i_{ds} + L_q w_r i_{qs} - L_d \dfrac{di_{ds}}{dt} \\ v_{qs} = -R_s i_{qs} - L_d w_r\, i_{ds} + w_r \lambda_r - L_q \dfrac{di_{qs}}{dt} \end{cases} \quad (11)$$

3. CONTROL ARCHITECTURE

3.1 Field-Oriented Control architecture

Among the advanced machine control techniques is vector control (or FOC) [19-26]. This control technique allows for the precise control of AC machines (such as PMSGs) by separately controlling torque and magnetic flux. This technique enables optimal and smooth machine operation. The control architecture is illustrated in Figure 3. Using the Park transformation, the currents (Ids and Iqs) and flux are controlled by PI controllers to precisely control the speed.

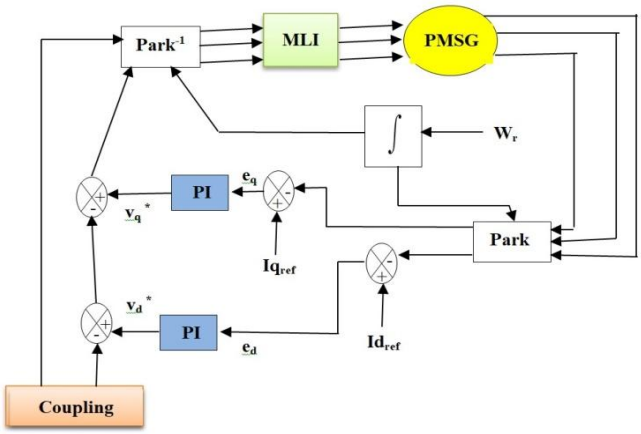

Figure 3. Field-Oriented Control (FOC) scheme

Recent work [27] demonstrates FOC applied to PV-fed dual open-end-winding induction drives with fuzzy FOC, evidencing FOC's continuing applicability in renewable-energy-driven electric-drive systems.

3.2 Integral Sliding Mode Control within Field-Oriented Control

In this study, Field-Oriented Integral Sliding Mode Control (FO-ISMC) is employed for the dq-axis current regulation of the WECS. FO-ISMC refers to the application of an ISMC within a FOC framework, allowing precise control of electromagnetic torque and flux, similar to the operation of a DC motor.

3.2.1 Conventional sliding mode control

The implementation of this control method requires mainly three stages:

Sliding surfaces: It has been proposed a form of general equation to determine the sliding surface [28].

With:

$$s(x,t) = \left(\frac{d}{dt} + \lambda\right)^{n-1} . e(t) \quad (12)$$

where, $e(t)$ is the error in the output state.

$$e(t) = x_{ref} - x(t) \quad (13)$$

where, n is a positive coefficient.

Conditions of convergence: The convergence condition is defined by the equation of Lyapunov:

$$s.\dot{s} < 0 \quad (14)$$

Controller design: Consequently, the structure of a controller consists of two parts; a first concerning the exact linearization and a second stabilizing.

$$u(t) = u_{eq}(t) + u_n \quad (15)$$

where, $n\, u_{eq}(t)$ corresponds to the equivalent control suggested, it is calculated on basis of the system, behavior along the sliding mode described by:

$$\dot{s}(x,t) = 0 \quad (16)$$

$$u_n = -K\, sgn(s) \quad (17)$$

where, $K > 0$, and it represents the control gain.

$$sgn(s) = \begin{cases} 1 & s > 0 \\ 0 & s = 0 \\ -1 & s < 0 \end{cases} \quad (18)$$

3.2.2 Integral Sliding Mode Control for dq-axis currents

The ISMC surface employed in this work is based on standard formulations [29], whose stability has been previously established. It is applied here to the dq-axis current regulation of the WECS. The purpose of this section is to present the design procedure of an ISMC for the system. The sliding surface for the dq-axis current control are:

$$\begin{cases} s_d(t) = e_d(t) + C_d \int e_d(t) dt \\ s_q(t) = e_q(t) + C_q \int e_q(t) dt \end{cases} \quad (19)$$

where, e_d and e_q are the direct and quadratic expressed as:

$$\begin{cases} e_d(t) = i_{ds} - i_{ds\_ref} \\ e_q(t) = i_{qs} - i_{qs\_ref} \end{cases} \quad (20)$$

Taking the time derivative on both sides of Eq. (20) leads to:

$$\begin{cases} \dot{s_d}(t) = \dot{e_d}(t) + C_d e_d(t) \\ \dot{s_q}(t) = \dot{e_q}(t) + C_q e_q(t) \end{cases} \quad (21)$$

where, k_d and k_q are positive constants.

$$\begin{cases} \dot{s}_d(t) = (\dot{\imath_{ds}} - \dot{\imath_{ds_{ref}}}) + C_d e_d(t) \\ \dot{s}_q(t) = (\dot{\imath_{qs}} - \dot{\imath_{qs_{ref}}}) + C_q e_q(t) \end{cases} \quad (22)$$

By Eqs. (10) and (22), we obtain:

$$\begin{cases} \dot{s}_d(t) = -\frac{R_s}{L_d} i_{ds} - \frac{1}{L_d} v_{ds} - \dot{i_{ds_{ref}}} + \dot{C}_d e_d(t) \\ \dot{s}_q(t) = -\frac{R_s}{L_q} i_{qs} - \frac{1}{L_q} v_{qs} - \dot{i_{qs_{ref}}} + C_q e_q(t) \end{cases} \quad (23)$$

Then, v_{ds} and v_{qs} are given by the same method as shown by:

$$\begin{cases} v_{ds} = -R_s i_{ds} - L_d \dot{\imath_{ds_{ref}}} + C_d L_d \, e_d(t) \\ \qquad -L_d \, K_d \, sgn(s(t)) \\ v_{qs} = -R_s i_{qs} - L_q \dot{\imath_{qs_{ref}}} + C_q L_q \, e_q(t) \\ \qquad -L_q \, K_q \, sgn(s(t)) \end{cases} \quad (24)$$

We will add the coupling terms:

$$\begin{cases} v_{ds} = -R_s i_{ds} - L_d \dot{\imath_{ds_{ref}}} + C_d L_d \, e_d(t) \\ \quad -L_d \, K_d \, sgn\big(s(t)\big) + L_q w_r \, i_{qs} \\ v_{qs} = -R_s i_{qs} - L_q \dot{\imath_{qs_{ref}}} + C_q L_q \, e_q(t) \\ -L_q \, K_q \, sgn\big(s(t)\big) + L_d w_r \, i_{qs} + w_r \, \lambda_r \end{cases} \quad (25)$$

4. METAHEURISTIC ALGORITHMS FOR OPTIMIZATION

Nature-inspired metaheuristic algorithms have emerged as some of the most powerful and versatile tools for addressing complex and high-dimensional optimization problems that are often nonlinear, non-convex, and involve multiple conflicting objectives. Inspired by biological, ecological, and physical processes observed in nature such as the foraging behavior of swarms, the evolutionary dynamics of natural selection, or the cooperative behavior of social animals these algorithms are particularly well-suited for problems where traditional deterministic methods fail or become computationally intractable.

Their ability to explore large and irregular search spaces, escape local optima, and adapt dynamically to changing optimization landscapes makes them ideal candidates for engineering applications, especially in control systems, energy systems, and robotics.

In recent years, these algorithms including PSO, Genetic Algorithms, GWO, Ant Colony Optimization (ACO), and others have demonstrated remarkable effectiveness in solving real-world problems where robustness, convergence speed, and solution diversity are critical [24]. Their flexibility allows for easy integration with problem-specific heuristics or hybridization with local search techniques, thereby enhancing both exploration and exploitation capabilities. Within the context of wind energy systems and advanced control design, such algorithms provide a robust framework for fine-tuning controller parameters to optimize system performance under uncertain, nonlinear, and time-varying conditions.

In this study, the optimization process was guided by a fitness function based on a scalarization approach to multi-objective optimization [30]. This approach converts a multi-objective problem into a single-objective formulation by combining the individual objective functions into a weighted sum, with coefficients w_1 and w_2 reflecting the relative importance of each objective. Consequently, each objective contributes proportionally to the overall evaluation, enabling the application of conventional single-objective optimization algorithms.

Four objective functions were considered in the optimization process, each highlighting a specific performance priority typically required in practical WECS controllers. The Absolute Integral Error (AIE) quantifies the global tracking accuracy of the d- and q-axis currents, independently of the error sign, making it suitable when the main concern is minimizing steady-state deviations. The Squared Integral Error (SIE) penalizes large instantaneous errors more severely, which is relevant in situations where significant current deviations may generate electromagnetic stress or deteriorate power quality. The Temporal Absolute Integral Error (TAIE) introduces a time-dependent weighting factor, assigning greater importance to errors that persist during the transient period; this reflects the practical need for rapid suppression of residual errors and the avoidance of slow convergence. Lastly, the Temporal Squared Integral Error (TSIE) combines both temporal and squared penalization effects, targeting late and large errors simultaneously, an essential consideration in real systems where prolonged deviations can induce thermal stress and reduce actuator lifetime.

Using these four objective functions therefore provides a comprehensive evaluation of the controller's performance in terms of tracking precision, mitigation of large deviations, transient response quality, and fast error extinction, aligning with the typical requirements of real WECS control.

The four objective functions are defined as follows:

$$AIE = w_1 \int |e_{d.norm}| dt + w_2 \int |e_{q.norm}| dt \quad (26)$$

$$SIE = w_1 \int {e_{d.norm}}^2 dt + w_2 \int {e_{q.norm}}^2 dt \quad (27)$$

$$TAIE = w_1 \int t * |e_{d.norm}| dt + w_2 \int t * |e_{q.norm}| dt \quad (28)$$

$$TSIE = w_1 \int t * {e_{d.norm}}^2 dt + w_2 \int t * {e_{q.norm}}^2 dt \quad (29)$$

where, $e_{d.norm}$ and $e_{q.norm}$ are the normalized direct and quadratic current respectively, w_1 and w_2 are the weights assigned to each objective and:

$$\sum_{i=1}^{2} w_i = 1 \quad (30)$$

Each objective function was tested under four scalarization configurations to assess the impact of weighting on optimization outcomes. Initially, a non-scalarized approach was applied with equal weights ($w_1 = w_2 = 1$). This was followed by a balanced scalarization with $w_1 = w_2 = 0.5$, and two asymmetric configurations with $w_1 = 0.75$ and $w_2 = 0.25$

and with $w_1 = 0.25$ and $w_2 = 0.75$. The selected weights were chosen to reflect the relative importance of the e_d and e_q errors, emphasizing the error that has the greatest influence on system performance under typical operating conditions. Moreover, the different weighting configurations were tested to explore the trade-offs between these two objectives, allowing an assessment of how prioritizing e_d or e_q affects the overall optimization results. In particular, asymmetric weights were used to amplify the contribution of the corresponding error in the overall objective function, providing a clearer understanding of its impact on the optimization outcomes. These tests enabled a comparative analysis of how varying weights influence the controller's performance and the optimization algorithm's efficiency. Figure 4 below represents the block diagram of the optimization process of the proposed ISMC–FOC.

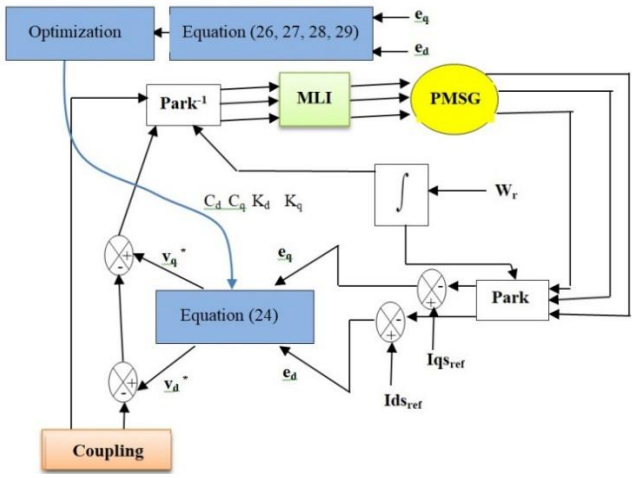

Figure 4. Block diagram of the proposed Field-Oriented Control (FOC) algorithm

The optimization loop interacts with the Simulink model automatically: at each iteration, the optimizer sends a new ISMC gain vector to the MATLAB workspace, and the model is executed through the *"sim"* command. The error signals produced by Simulink are saved using *To File* blocks and then reloaded in the script to compute the objective function. This bidirectional exchange allows evaluating each parameter set and guiding the optimizer toward the optimal solution.

4.1 Particle Swarm Optimization

PSO is an evolutionary computation technique inspired by the collective behavior of bird flocks and fish schools [31]. Each particle adjusts its position in the search space based on its own experience and that of its neighbors. For a detailed description of the algorithm and its mathematical formulation, the reader is referred to [31].

4.2 Grey Wolf Optimizer

GWO is a nature-inspired metaheuristic algorithm mimicking the social hierarchy and hunting behavior of grey wolves [23, 32]. The algorithm classifies solutions into α, β, δ, and ω categories to guide exploration and exploitation in the search space. For a complete description of the GWO algorithm and its mathematical details can be found in studies [23, 32].

4.3 Hybrid Particle Swarm Optimization algorithm

Most conventional meta-heuristic methods share some common features: they are nature-inspired, randomly initialized, and dependent on multiple input parameters that must be tuned according to the specific problem. However, despite their strengths, these algorithms also face several limitations, including long computational times, slow convergence rates, challenges with high-dimensional problems, and the absence of guarantees for achieving global optimality. Additionally, they often require substantial computational resources. According to the 'No-Free-Lunch' theorem, no single meta-heuristic algorithm can perform optimally across all types of optimization problems, which implies that there is always room for further improvement and innovation in this field [24].

4.3.1 Hybrid PSO-*fmincon* algorithm

Introduction to the *fmincon* function: *fmincon* is a nonlinear optimization function integrated into MATLAB, specifically designed to solve constrained problems (equality constraints, inequality constraints, variable bounds, etc.). It is widely used across various engineering and research fields for applications such as parameter estimation, system optimization, and the design of complex structures. Due to its effectiveness in finding local minima while satisfying imposed constraints, *fmincon* is considered a reliable tool for handling both precise and complex optimization problems [33].

Combined strategy and optimization workflow: The developed hybrid method combines the PSO algorithm with the *fmincon* function. This combination aims to leverage the respective strengths of both approaches to achieve an optimal estimation of parameters within a constrained framework. PSO algorithm is initially employed to globally explore the search space. Thanks to its ability to generate a diverse population of solutions, it can quickly identify promising regions in the optimization domain. This global search phase ensures broad coverage of the solution space and helps avoid premature convergence to local minima. After this exploration phase, the best candidate solutions are passed on to *fmincon*, which performs a local refinement.

At this stage, the goal is to fine-tune the results obtained by PSO, ensuring precise satisfaction of the constraints and accelerating convergence towards a high-quality local optimum. This hybrid approach combines the strengths of global exploration and local optimization in a structured sequence. It begins with an exploration phase where the PSO algorithm generates and evaluates a population of solutions within the feasible space, followed by the selection of the most promising candidates. Then, the local optimizer *fmincon* is applied to these solutions to refine the results while respecting all constraints. Thanks to the complementarity between the exploratory capabilities of PSO and the precision of *fmincon*, this method provides a well-balanced trade-off between global exploration and local exploitation, making it particularly effective for solving complex and highly constrained problems.

4.3.2 Hybrid Particle Swarm Optimization–Grey Wolf Optimizer algorithm

Hybrid Particle Swarm Optimization–Grey Wolf Optimizer (HPSO–GWO) algorithm is a novel swarm-based metaheuristic algorithm that offers several advantages, including ease of implementation and low memory

requirements. Its core idea lies in combining the strong exploitation capability of PSO with the effective exploration behavior of the GWO [34-39]. By integrating the strengths of both approaches, the hybrid algorithm enhances performance while maintaining efficient memory usage [20]. Notably, HPSO–GWO operates in a coevolutionary manner, meaning that PSO and GWO components evolve in parallel rather than sequentially. This parallel structure contributes to a more balanced search process across the solution space. Unlike conventional methods that rely on traditional mathematical formulations, HPSO–GWO updates the positions of the top three agents in the search space using a hybridized mechanism [24]. The flowchart of hybrid PSO–GWO algorithm is illustrated by the following Figure 5 [39].

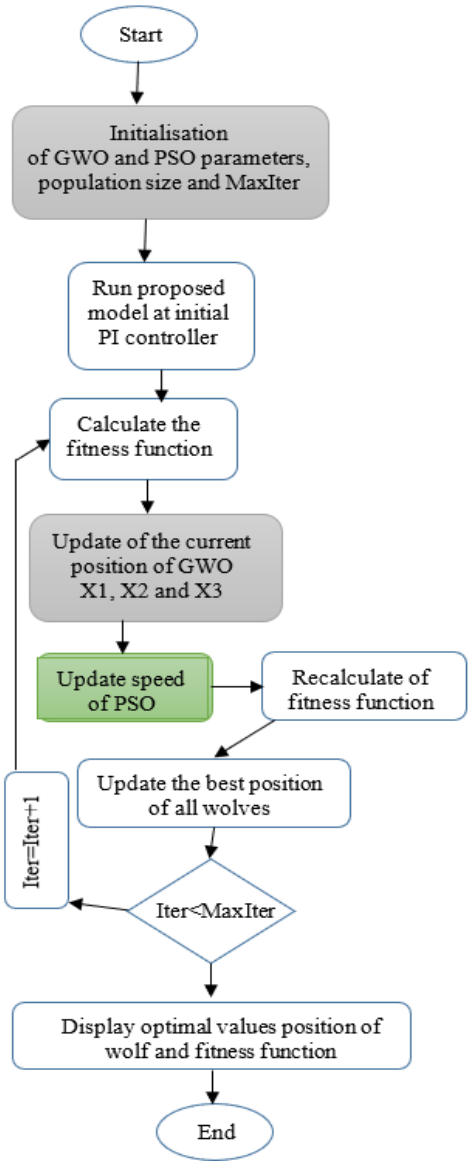

Figure 5. Flowchart for hybrid Particle Swarm Optimization–Grey Wolf Optimizer (HPSO–GWO) algorithm [39]

5. SIMULATION RESULTS AND DISCUSSION

The simulation experiments were conducted in MATLAB/Simulink to evaluate and enhance the performance of the Integral Sliding Mode Flow-Oriented Controller (ISMFOC) for wind turbine speed regulation. To optimize the controller parameters, several optimization strategies were employed, including PSO, the hybrid PSO-*fmincon* approach, the GWO, and the hybrid PSO–GWO algorithm. The algorithm parameters were determined after several preliminary experiments to achieve a good compromise between convergence speed, robustness, and computational effort.

For both the PSO and GWO algorithms, as well as their hybrid variants (PSO-*fmincon* and PSO–GWO), we used a population size of 50 and a maximum of 50 iterations. In PSO, the inertia weight w was set to decrease linearly from 0.9 to 0.4, while the cognitive and social acceleration coefficients were fixed to $c_1 = c_2 = 2$. In GWO, the convergence control parameter a decreased linearly from 2 to 0, with the encircling coefficients A and C computed as in the original formulation. Finally, all simulations were performed with a fixed Simulink step size of 10^{-3}.

These parameter settings were validated through sensitivity analyses and repeated trials, which confirmed their effectiveness and stability for the studied control problem. The variable wind profile used in the simulations is depicted in Figure 6.

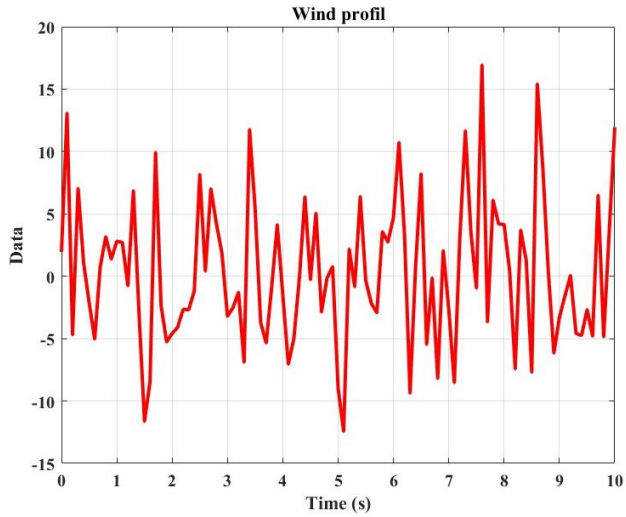

Figure 6. Variable wind profile

5.1 Simulation 01: Flow-oriented integral sliding mode control

The detailed results obtained with the FO-ISMC are presented in Figures 7-10.

The results indicate (Figure 7) that the system operates effectively under both transient and steady-state conditions, with an observed error of 0.2 and a response time of 4.5×10^{-3} s, and without any overshoot. Figure 8 presents the direct-axis current response obtained with the same ISMC controller, where a noticeable chattering phenomenon appears around the zero direct current value.

For the active power, the results shown in Figure 9 highlight the necessity of employing optimization techniques to determine suitable controller parameters, given the significant tracking error observed.

Figure 10 displays the tracking errors of the quadrature current (blue) and the direct current (red) with respect to their corresponding reference values.

The quadrature current error reaches a value of 0.2, whereas the direct current error remains extremely small, oscillating around zero with an amplitude on the order of 5×10^{-6}.

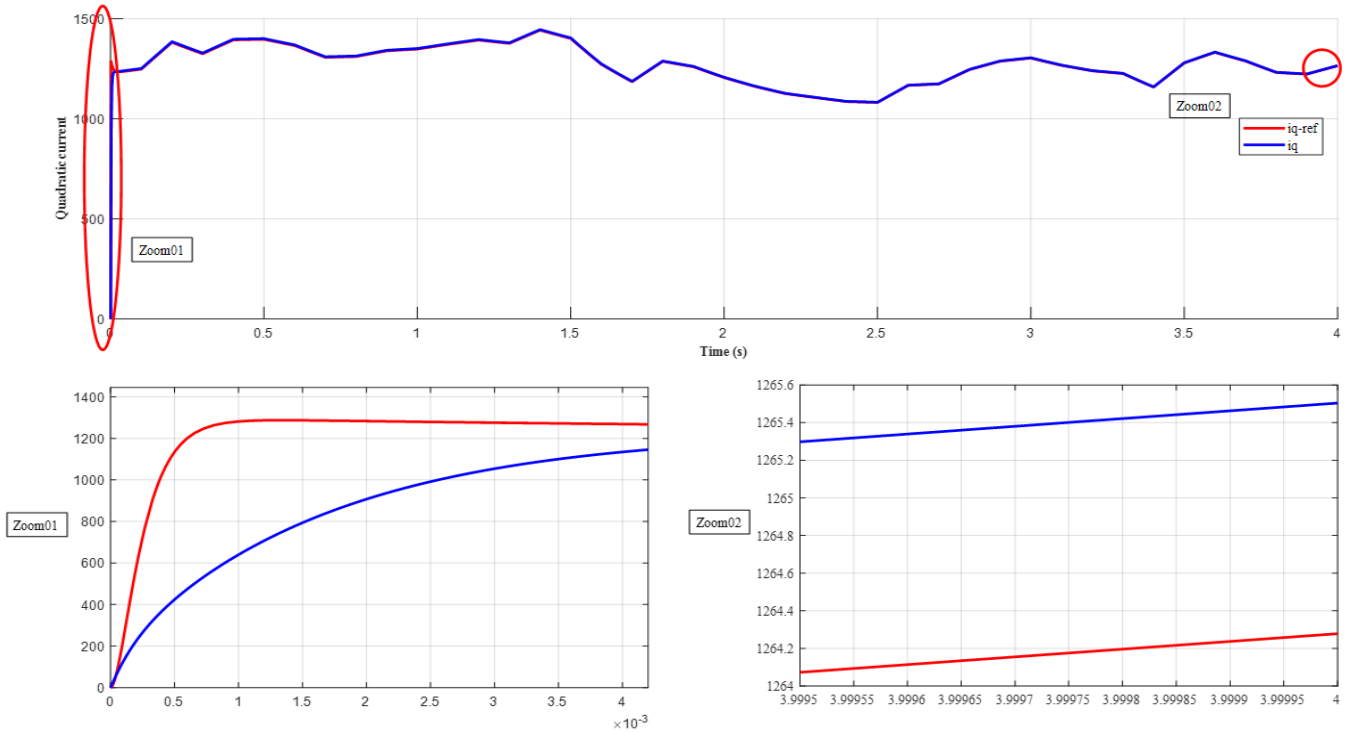

Figure 7. Quadratic current

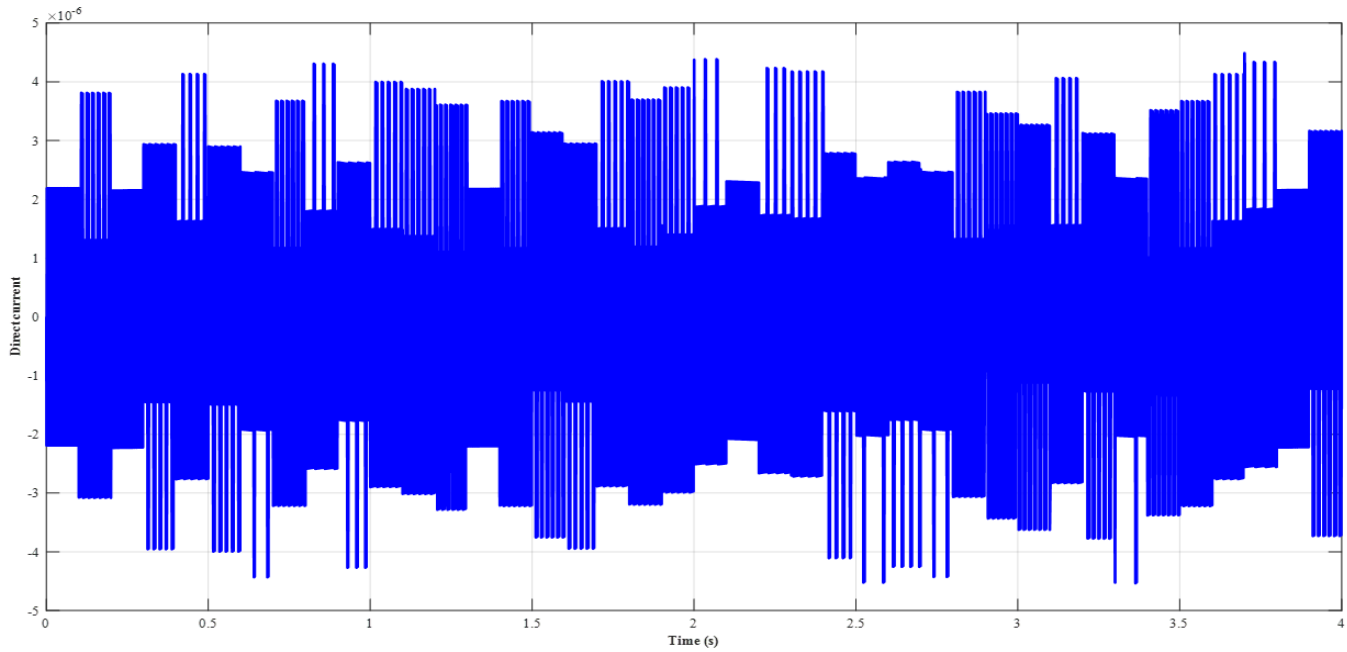

Figure 8. Direct current

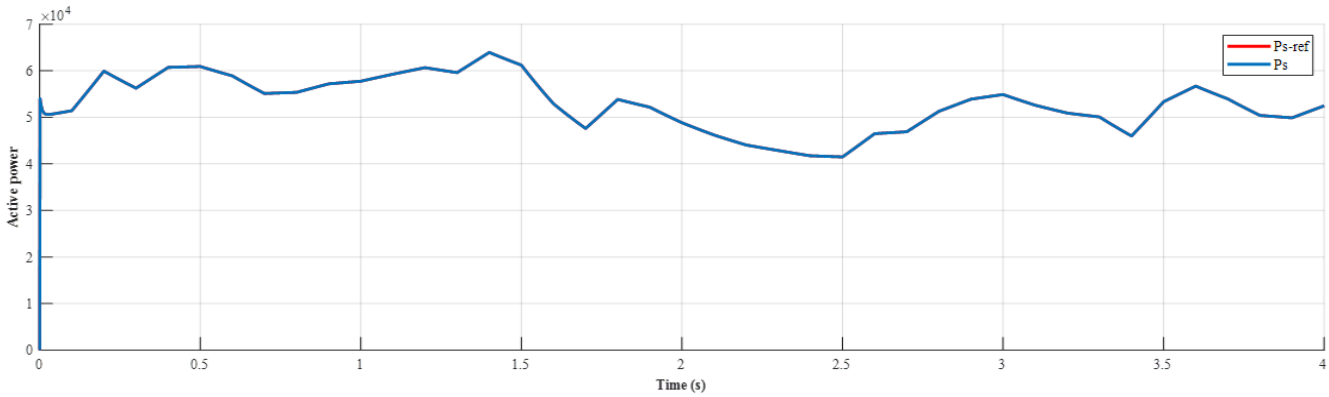

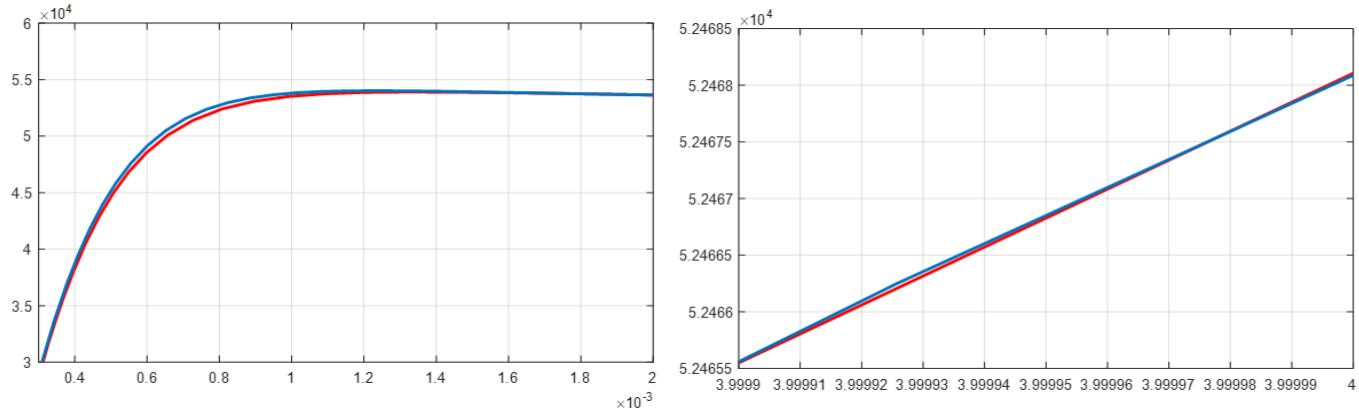

Figure 9. Active power

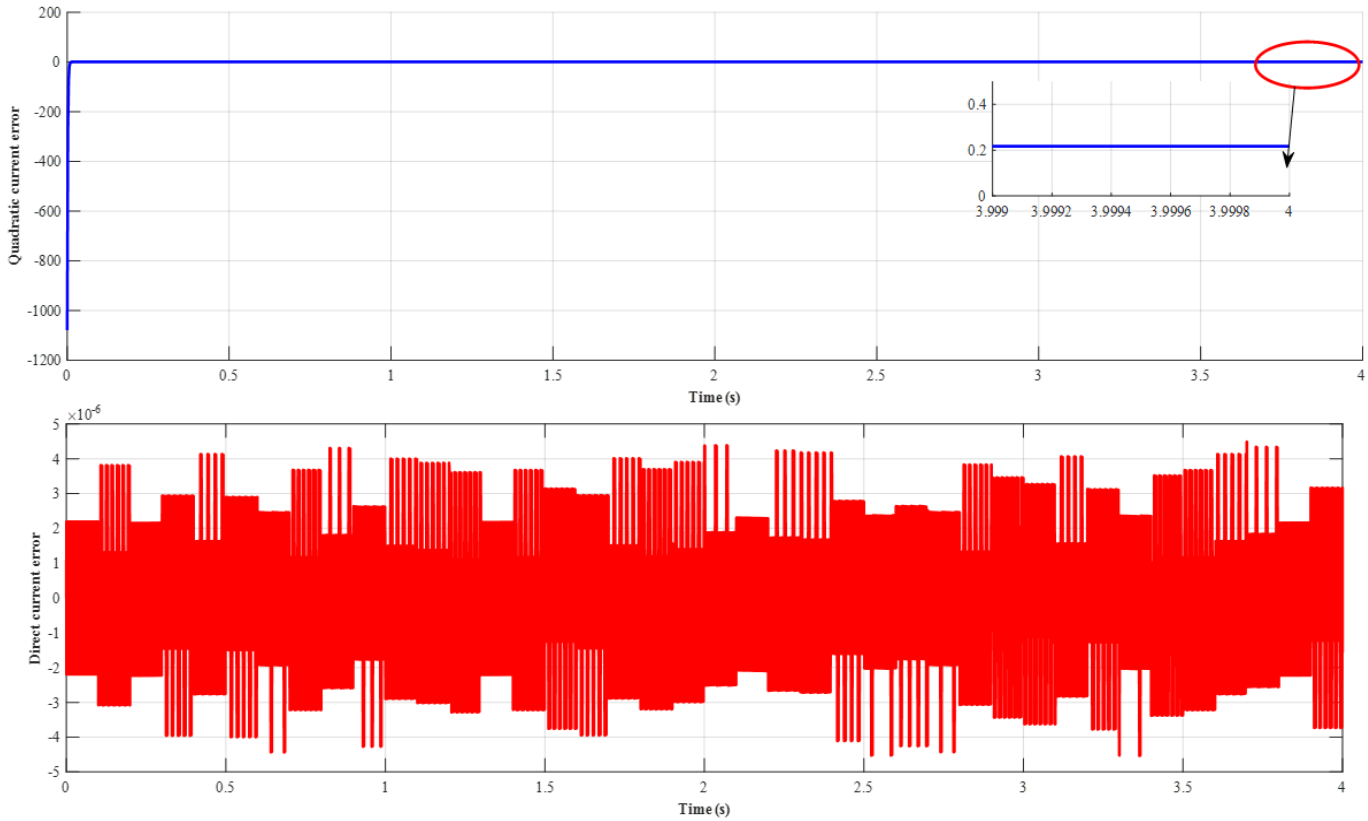

Figure 10. Quadratic and direct current errors

Table 1. The obtained results with Particle Swarm Optimization (PSO) algorithm

Fitness Function	Weights	Time	e_d	e_q
Absolute Integral Error (AIE)	$w_1 = 1\ w_2 = 1$	$1.48e^{+04}$	3.25×10^{-6}	5.56×10^{-3}
	$w_1 = 0.5\ w_2 = 0.5$	$8.31e^{+03}$	3.01×10^{-6}	-2.07×10^{-2}
	$w_1 = 0.25\ w_2 = 0.75$	$1.05e^{+04}$	3.86×10^{-6}	1.79×10^{-3}
	$w_1 = 0.75\ w_2 = 0.25$	$1.18e^{+04}$	8×10^{-6}	-1.62×10^{-2}
Squared Integral Error (SIE)	$w_1 = 1\ w_2 = 1$	$3.28e^{+03}$	2.5×10^{-7}	3.21×10^{-3}
	$w_1 = 0.5\ w_2 = 0.5$	$2.84e^{+03}$	2.79×10^{-7}	-9.23×10^{-3}
	$w_1 = 0.25\ w_2 = 0.75$	$3.17e^{+03}$	2.78×10^{-7}	-5.52×10^{-3}
	$w_1 = 0.75\ w_2 = 0.25$	$2.05e^{+04}$	-4.13×10^{-8}	1.54×10^{-2}
Temporal Absolute Integral Error (TAIE)	$w_1 = 1\ w_2 = 1$	$5.46e^{+3}$	3.05×10^{-6}	3.16×10^{-2}
	$w_1 = 0.5\ w_2 = 0.5$	$5.04e^{+3}$	-2.111×10^{-6}	2.38×10^{-2}
	$w_1 = 0.25\ w_2 = 0.75$	$5.30e^{+3}$	3.65×10^{-6}	3.4×10^{-2}
	$w_1 = 0.75\ w_2 = 0.25$	$4.16e^{+3}$	-4.84×10^{-7}	2.15×10^{-2}
Temporal Squared Integral Error (TSIE)	$w_1 = 1\ w_2 = 1$	$1.75e^{+4}$	-2.92×10^{-7}	-1.67×10^{-2}
	$w_1 = 0.5\ w_2 = 0.5$	$3.21e^{+3}$	3.07×10^{-7}	-1.535×10^{-4}
	$w_1 = 0.25\ w_2 = 0.75$	$2.32e^{+3}$	3.07×10^{-7}	-1.533×10^{-4}
	$w_1 = 0.75\ w_2 = 0.25$	$1.15e^{+3}$	-3.08×10^{-7}	1.42×10^{-3}

5.2 Simulation 02: Particle Swarm Optimization algorithm

The detailed results obtained using the PSO algorithm under various fitness functions and weighting combinations are summarized in the following table, highlighting the impact of each configuration on computation time, tracking direct and quadratic errors (e_d and e_q), and minimizing chattering. Table 1 illustrates the obtained results.

Among all tested configurations, the combination using the TSIE fitness function with $w_1 = 0.25$ and $w_2 = 0.75$ stands out as the most efficient and well-balanced. This asymmetric weighting, which emphasizes the minimization of the quadratic error (e_q) and the direct error (e_d) in levels of ($\sim 10^{-7}$) and a remarkable 60% decrease in computation time compared to the AIE-based approach. These results demonstrate that this configuration offers the most reliable compromise between accuracy and efficiency. The results corresponding to the optimal configuration are illustrated in Figures 11-14. Figure 11 illustrates the quadratic current curve obtained using the hybrid PSO–ISMC approach alongside its reference.

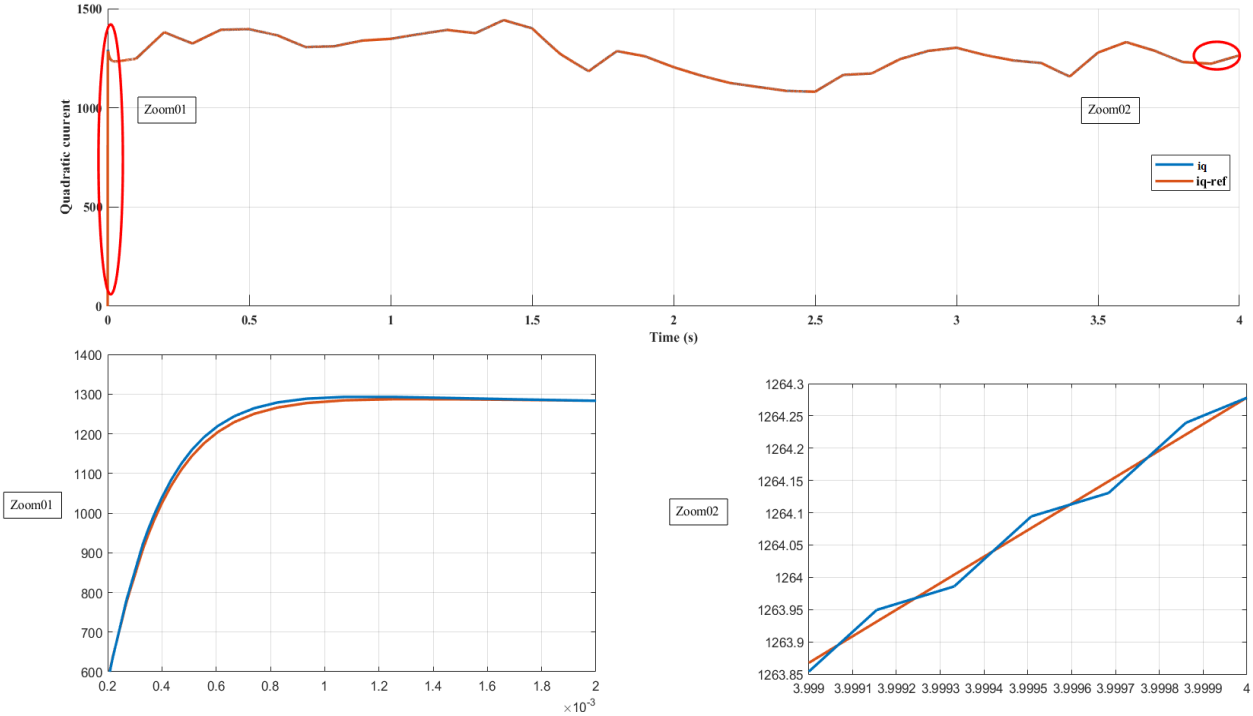

Figure 11. Quadratic current

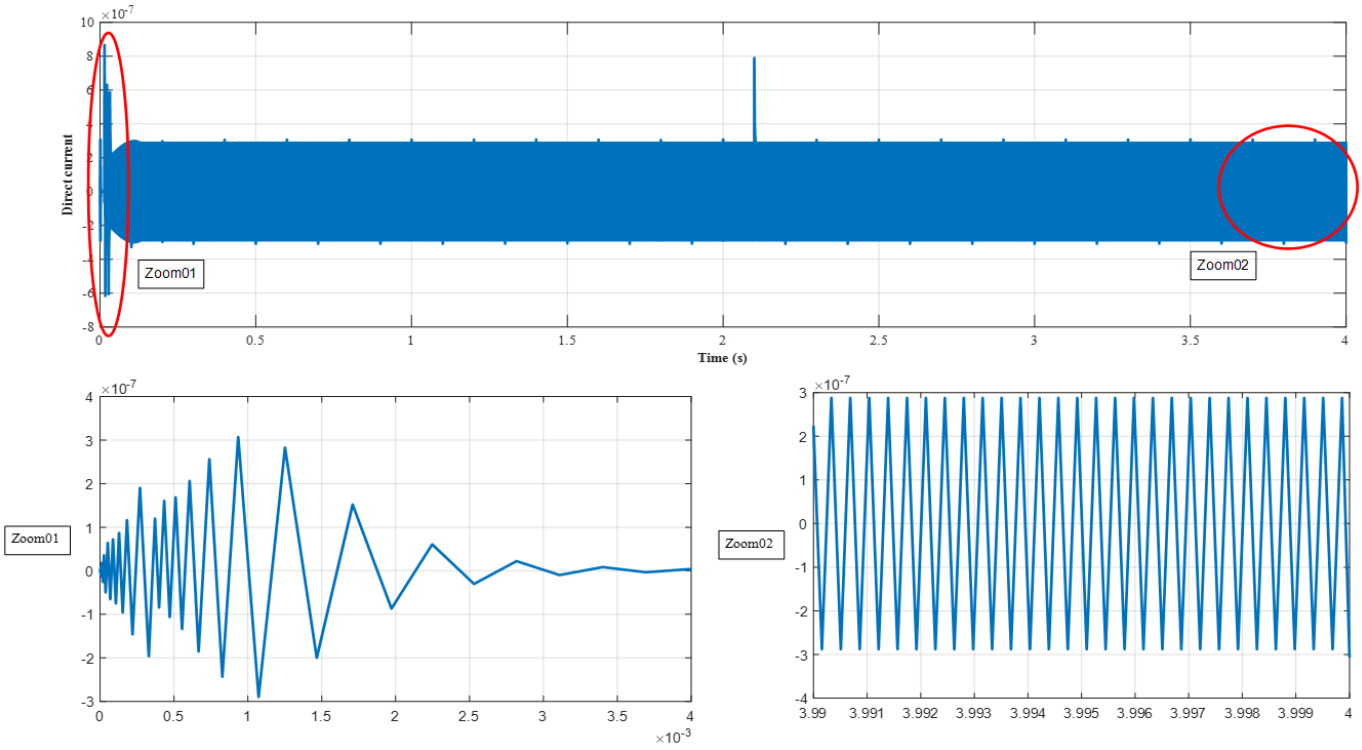

Figure 12. Direct current

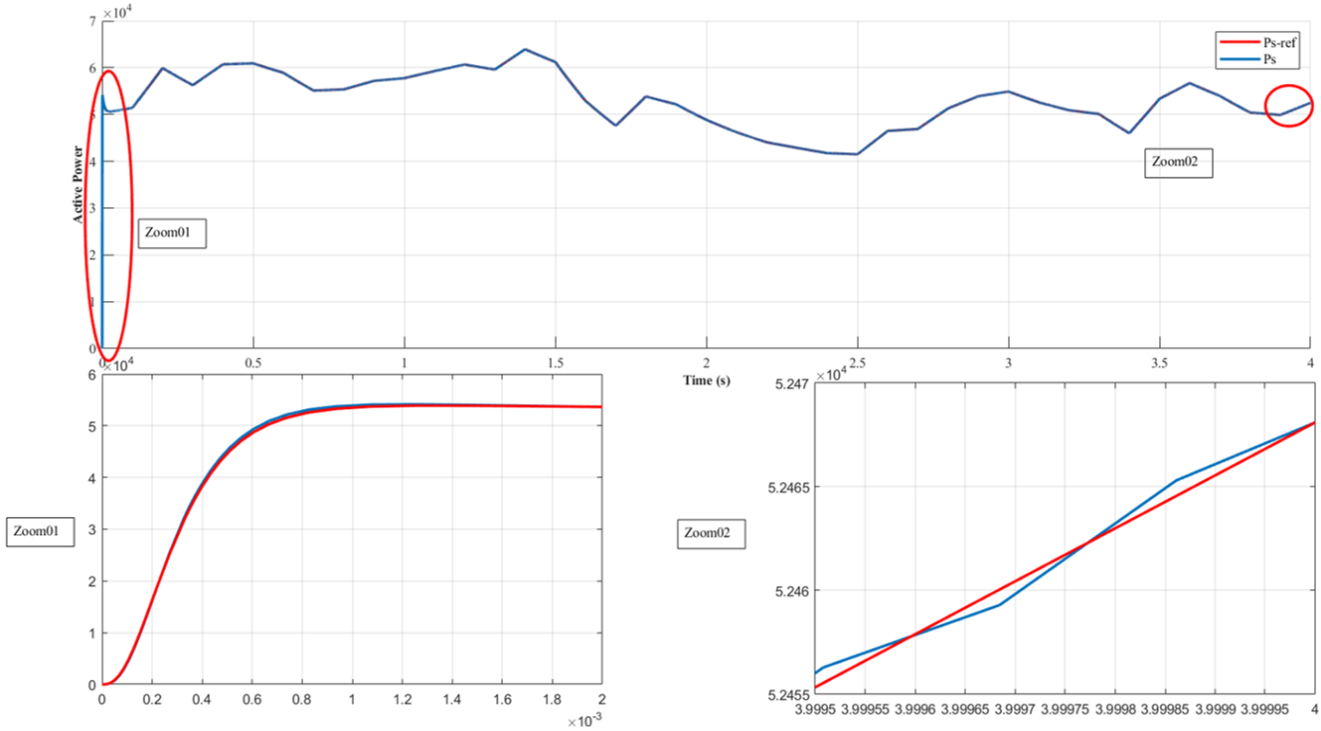

Figure 13. Active power

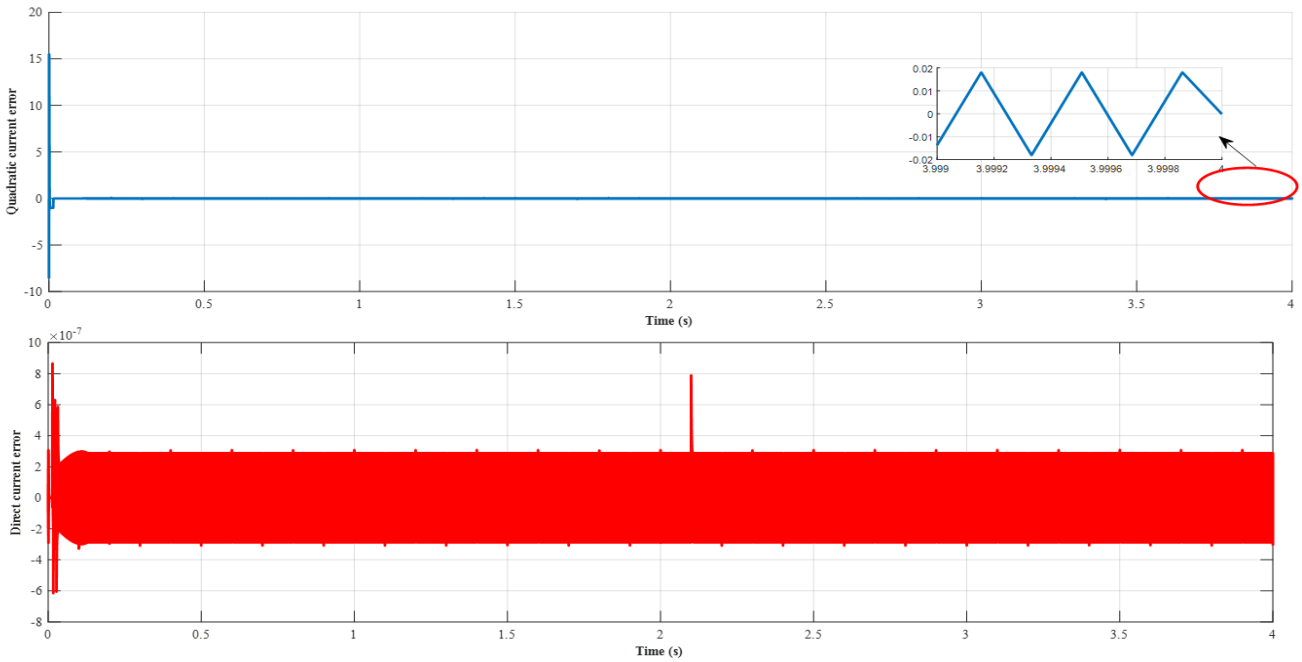

Figure 14. Quadratic and direct current errors

After the rising phase, the current reaches a maximum peak of approximately 1292.78 yielding an absolute overshoot of about 5.69 A, corresponding to ≈ 0.44% of the final value. The observed settling time is 1.65×10^{-3}. The steady-state error is 1.533×10^{-4}, confirming a virtually null deviation from the reference. Moreover, the zoomed view highlights that the chattering around the reference value is extremely limited, with only very small amplitude oscillations, indicating that the hybrid PSO–ISMC controller effectively mitigates the classical high-frequency switching behavior typically associated with sliding-mode control. Figure 12 shows the direct current response under the hybrid PSO–ISMC approach. Minimal chattering is observed around the reference value of zero, with an extremely small steady-state error of 3.07×10^{-7}.

For the active power, the results presented in Figure 13 confirm the effectiveness of the proposed approach in minimizing the tracking error, with only minimal chattering observed. Figure 14 presents the tracking errors of both the quadratic current (shown in blue) and the direct current (shown in red) relative to their respective reference values.

The quadratic current error exhibits small oscillations around zero with an amplitude of approximately 0.02, while the direct current error remains extremely low, fluctuating around zero with an amplitude on the order of 3×10^{-7}. These results highlight the high precision of the proposed control strategy in maintaining accurate current regulation.

5.3 Simulation 03: Hybrid Particle Swarm Optimization-*fmincon*

Table 2 provides a comparative overview of the performance of various fitness functions and weights applied with the hybrid PSO-*fmincon* algorithm allowing an evaluation of their impact on control accuracy and efficiency.

The PSO-*fmincon* hybridization applied to the AIE fitness function with equal weighting ($w_1 = w_2 = 1$) demonstrates very high precision, achieving $e_d \approx 10^{-6}$ and $e_q \approx 0.001821$. However, this configuration requires a relatively longer computation time compared to the one using TSIE with $w_1 = 0.25$ and $w_2 = 0.75$, which provides a better trade-off between accuracy and computational efficiency. This latter setup achieves excellent performance ($e_d \approx 9.35 \times 10^{-7}$, $e_q \approx 0.002727$) with a reasonable execution time (≈ 4018 s), making it the most balanced and globally optimal result in terms of precision and efficiency. Figures 15-18 present the results obtained using the most effective configuration identified.

Figure 15 shows the quadratic current response using the hybrid PSO-*fmincon*–ISMC method, compared to its reference.

Following the rising phase, the current attains a peak of approximately 1292.11 A, resulting in an absolute overshoot of around 5.02 A, which corresponds to roughly 0.39% of the final value. The settling time is observed to be 1.6×10^{-3} s, while the steady-state error is only 2.72×10^{-3}, indicating an almost negligible deviation from the reference. Additionally, the zoomed-in view shows that chattering around the reference is minimal, with only very small oscillations, demonstrating the effectiveness of the hybrid PSO–ISMC controller.

Figure 16 illustrates the direct current response under the proposed control strategy, revealing a narrow chattering band with occasional small-amplitude peaks with an extremely small steady-state error of 2.64×10^{-6}.

Table 2. The obtained results with hybrid Particle Swarm Optimization (PSO)-*fmincon* algorithm

Fitness Function	Weights	Time	e_d	e_q
Absolute Integral Error (AIE)	$w_1 = 1$ $w_2 = 1$	$9.05e^{+3}$	-2.64×10^{-6}	-1.82×10^{-3}
	$w_1 = 0.5$ $w_2 = 0.5$	$1.5e^{+4}$	-1.77×10^{-6}	-3.84×10^{-2}
	$w_1 = 0.25$ $w_2 = 0.75$	$9.69e^{+3}$	-1.76×10^{-6}	-3.04×10^{-2}
	$w_1 = 0.75$ $w_2 = 0.25$	$9.59e^{+3}$	-6.77×10^{-7}	-1.82×10^{-2}
Squared Integral Error (SIE)	$w_1 = 1$ $w_2 = 1$	$6.45e^{+3}$	2.67×10^{-7}	3.50×10^{-3}
	$w_1 = 0.5$ $w_2 = 0.5$	$5.98e^{+3}$	-1.77×10^{-7}	-1.26×10^{-2}
	$w_1 = 0.25$ $w_2 = 0.75$	$4.01e^{+3}$	7.14×10^{-7}	6.86×10^{-3}
	$w_1 = 0.75$ $w_2 = 0.25$	$3.38e^{+3}$	-7.06×10^{-7}	5.80×10^{-3}
Temporal Absolute Integral Error (TAIE)	$w_1 = 1$ $w_2 = 1$	$6.09e^{+3}$	-2.36×10^{-6}	-1.74×10^{-2}
	$w_1 = 0.5$ $w_2 = 0.5$	$6.45e^{+3}$	2.11×10^{-6}	-2.82×10^{-2}
	$w_1 = 0.25$ $w_2 = 0.75$	$5.18e^{+3}$	-2.52×10^{-6}	-2.84×10^{-2}
	$w_1 = 0.75$ $w_2 = 0.25$	$7.12e^{+3}$	-3×10^{-6}	-1.59×10^{-2}
Temporal Squared Integral Error (TSIE)	$w_1 = 1$ $w_2 = 1$	$5.05e^{+3}$	4.30×10^{-8}	-6.3×10^{-3}
	$w_1 = 0.5$ $w_2 = 0.5$	$3.02e^{+3}$	9.50×10^{-8}	2.08×10^{-2}
	$w_1 = 0.25$ $w_2 = 0.75$	$4.01e^{+3}$	9.35×10^{-7}	2.72×10^{-3}
	$w_1 = 0.75$ $w_2 = 0.25$	$1.26e^{+3}$	3.34×10^{-7}	-7.14×10^{-3}

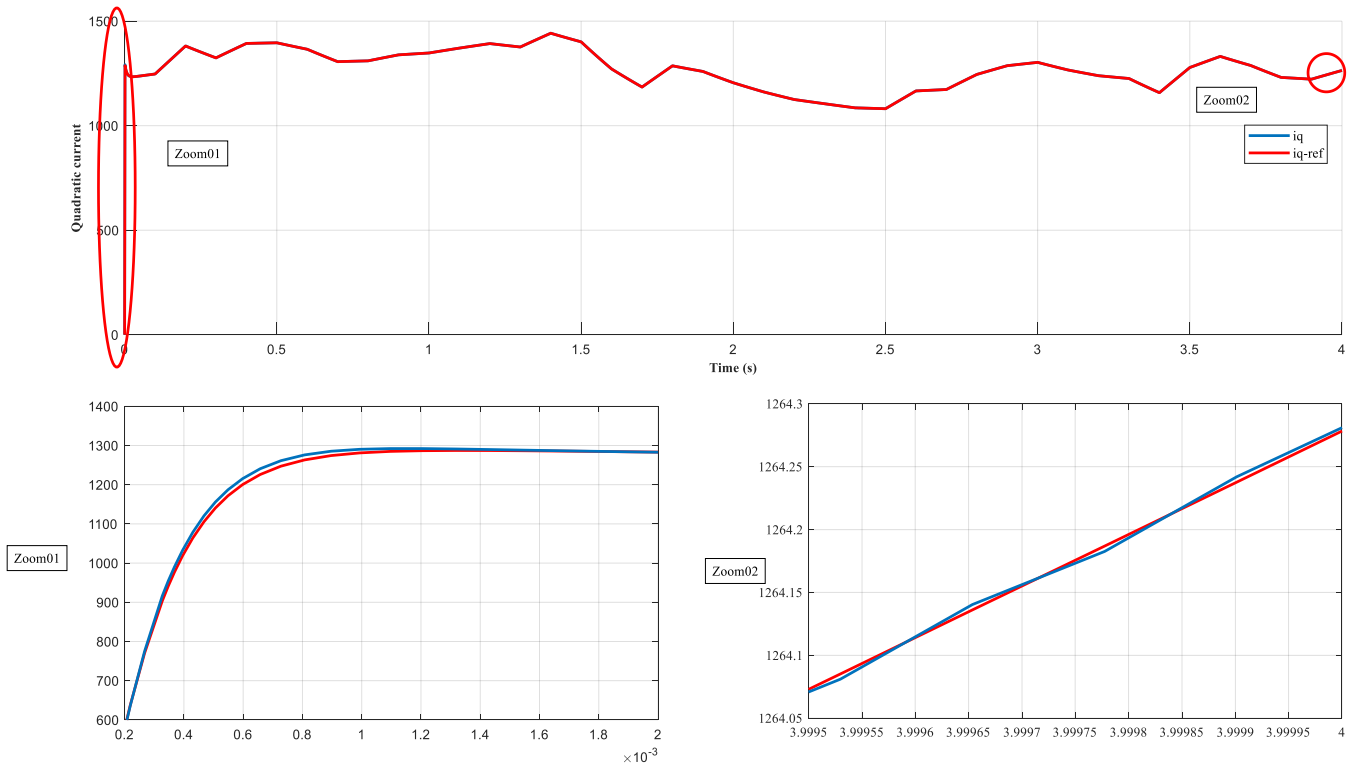

Figure 15. Quadratic current

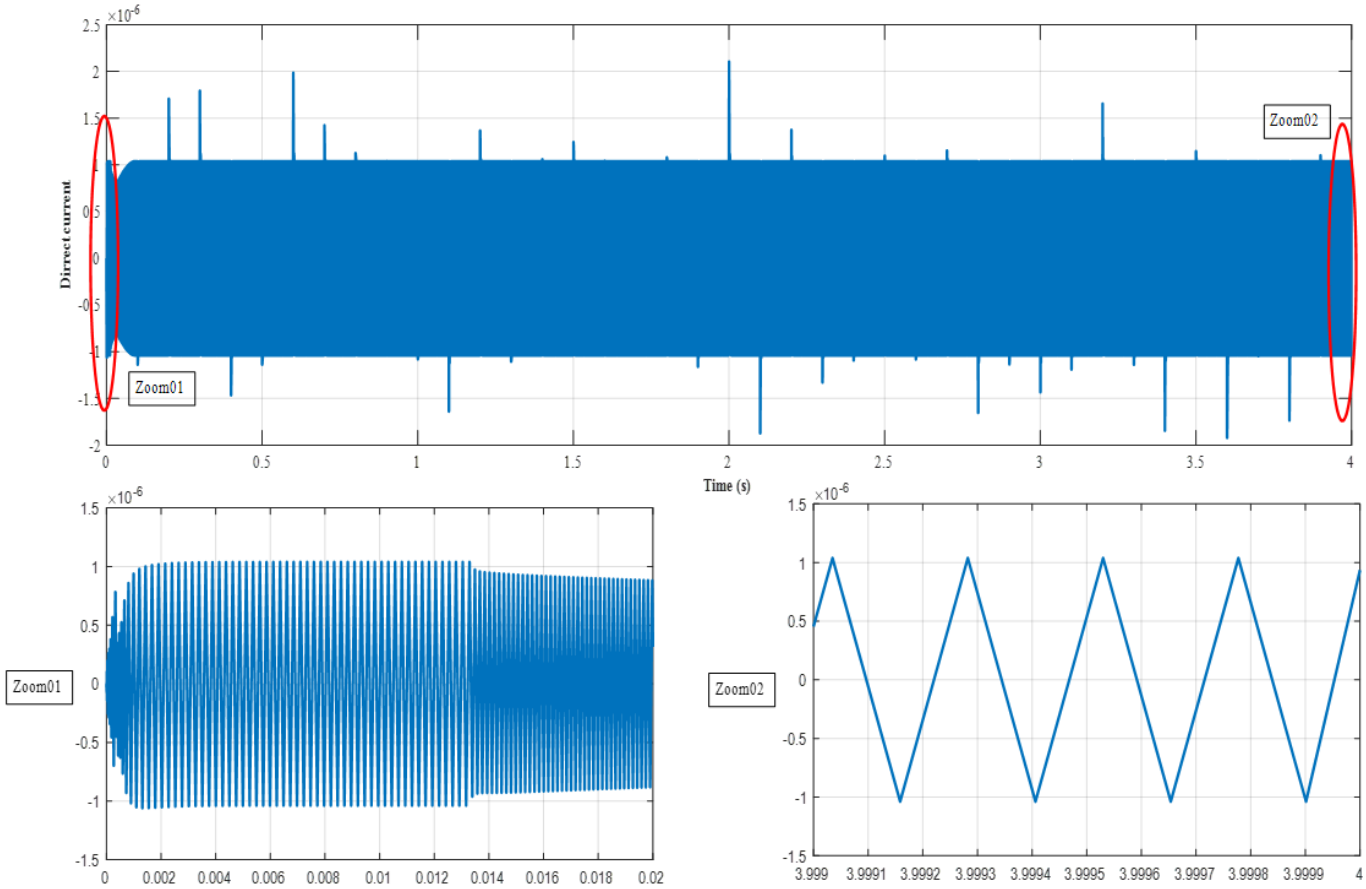

Figure 16. Direct current

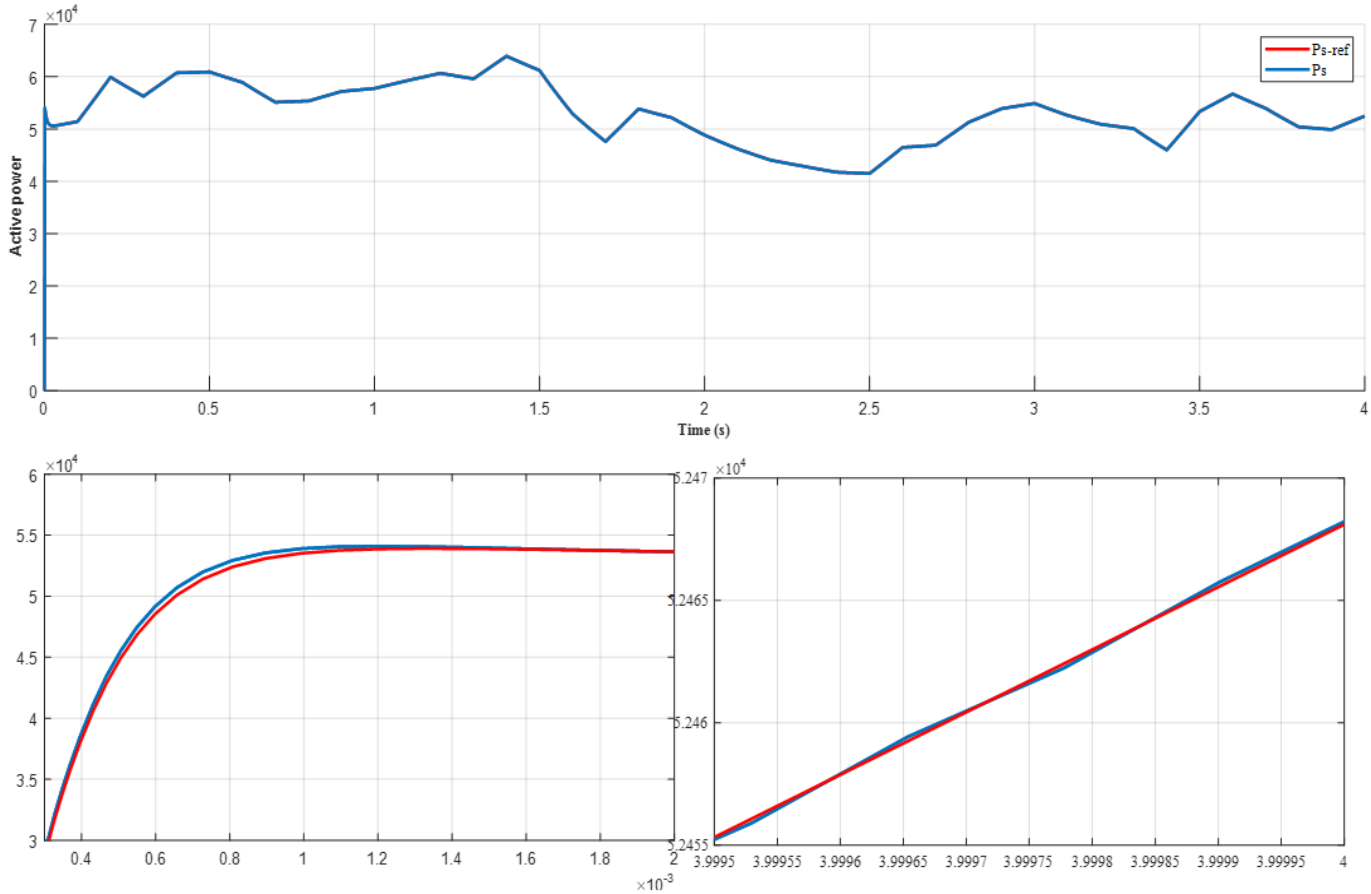

Figure 17. Active power

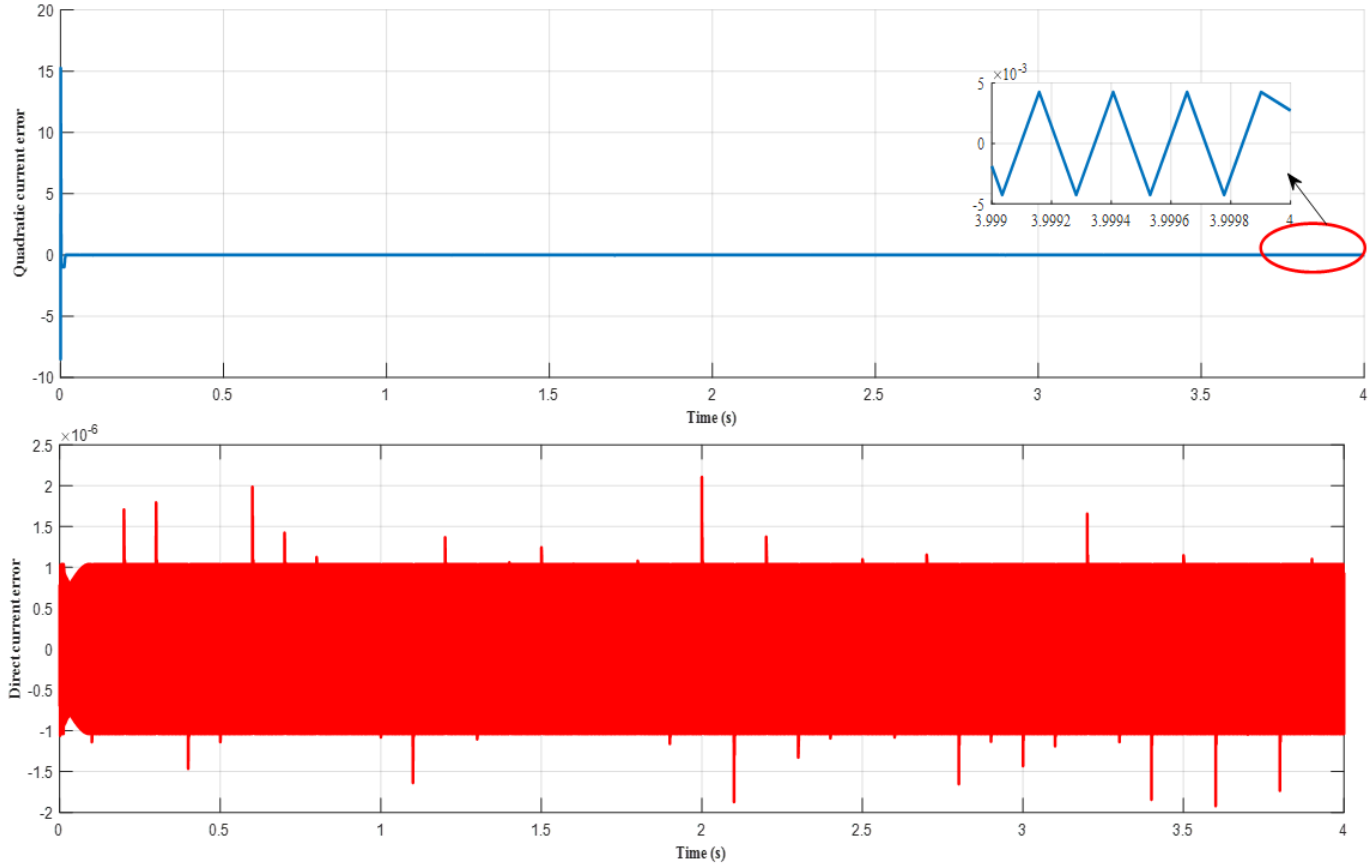

Figure 18. Quadratic and direct current errors

Table 3. The obtained results with Grey Wolf Optimizer (GWO) algorithm

Fitness Function	Weights	Time	e_d	e_q
Absolute Integral Error (AIE)	$w_1 = 1$ $w_2 = 1$	$2.91e^{+3}$	2.62×10^{-7}	-8.53×10^{-3}
	$w_1 = 0.5$ $w_2 = 0.5$	$2.22e^{+3}$	-1.27×10^{-7}	-1.32×10^{-2}
	$w_1 = 0.25$ $w_2 = 0.75$	$2.86e^{+3}$	-1.20×10^{-8}	-0.001224
	$w_1 = 0.75$ $w_2 = 0.25$	$2.84e^{+3}$	3.18×10^{-7}	-8.04×10^{-5}
Squared Integral Error (SIE)	$w_1 = 1$ $w_2 = 1$	$4.22e^{+3}$	-5.59×10^{-7}	-0.002195
	$w_1 = 0.5$ $w_2 = 0.5$	$4.2232e^{+3}$	-4.26×10^{-7}	0.0008014
	$w_1 = 0.25$ $w_2 = 0.75$	$2.99e^{+3}$	2.26×10^{-7}	0.001379
	$w_1 = 0.75$ $w_2 = 0.25$	$2.68e^{+3}$	1.09×10^{-7}	0.0005071
Temporal Absolute Integral Error (TAIE)	$w_1 = 1$ $w_2 = 1$	$2.33e^{+3}$	-2.94×10^{-7}	0.001347
	$w_1 = 0.5$ $w_2 = 0.5$	$2.22e^{+3}$	-3.19×10^{-7}	-0.001999
	$w_1 = 0.25$ $w_2 = 0.75$	$4.15e^{+3}$	2.46×10^{-7}	0.00222
	$w_1 = 0.75$ $w_2 = 0.25$	$2.29e^{+3}$	-5.46×10^{-7}	0.002865
Temporal Squared Integral Error (TSIE)	$w_1 = 1$ $w_2 = 1$	$2.35e^{+3}$	-1.30×10^{-6}	-6.04×10^{-4}
	$w_1 = 0.5$ $w_2 = 0.5$	$2.33e^{+3}$	-6.81×10^{-7}	2.36×10^{-3}
	$w_1 = 0.25$ $w_2 = 0.75$	$2.27e^{+3}$	2.90×10^{-7}	1.92×10^{-3}
	$w_1 = 0.75$ $w_2 = 0.25$	$2.21e^{+3}$	2.46×10^{-7}	2.22×10^{-3}

These slight deviations are primarily induced by wind speed fluctuations and remain well within acceptable limits, confirming the robustness and stability of the control system under variable operating conditions.

Figure 17 clearly illustrates the effectiveness of the PSO-*fmincon*–ISMC approach in precisely tracking the reference power, confirming its high control accuracy.

The direct current error (shown in red) and quadratic current error (shown in blue) are shown in Figure 18.

The direct current error fluctuates near zero with an amplitude of about 10^{-6}, however there are a few transient peaks. While the quadratic current error exhibits minor oscillations about zero with an amplitude of about 5×10^{-3}.

5.4 Simulation 04: Grey Wolf Optimizer

Table 3 highlights the performance metrics of the GWO algorithm under different fitness function and weighting strategies, helping to validate the relevance of each configuration in terms of precision and computational cost.

GWO emerges as the fastest algorithm, with an average computation time of approximately 2.3×10^3 s, highlighting its rapid convergence capability. Among all tested configurations, the one based on the TSIE fitness function with weights $w_1 = 0.25$ and $w_2 = 0.75$ proves to be the most effective. It achieves a well-balanced trade-off between error minimization (e_d and e_q) and computational efficiency, making it an optimal choice for applications requiring a balance

between robustness reduced computational cost. The results achieved with the most performant configuration are displayed in the Figures 19-22, highlighting its superior behavior.

Figure 19 presents the quadratic current response obtained using the hybrid GWO–ISMC method along with its reference.

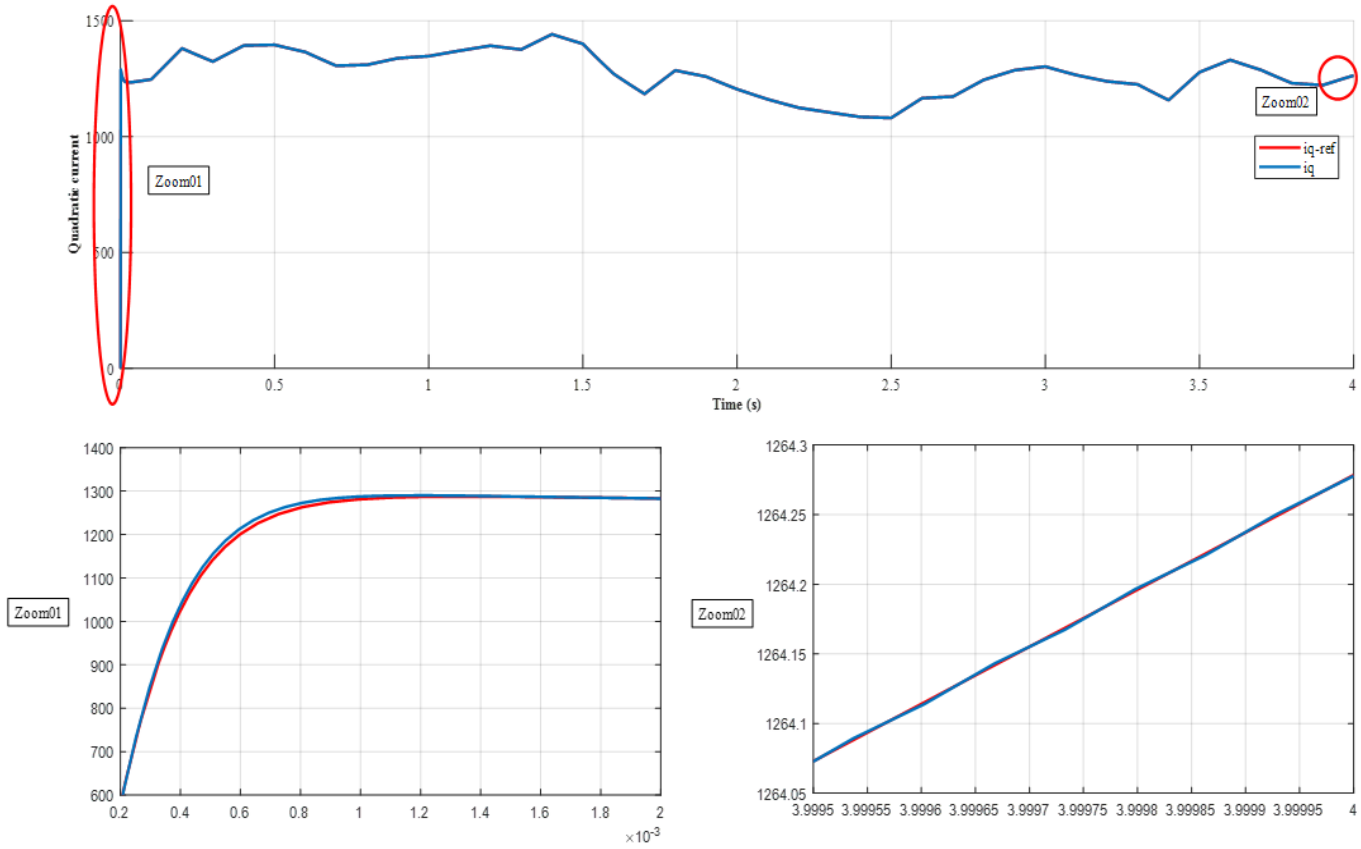

Figure 19. Quadratic current

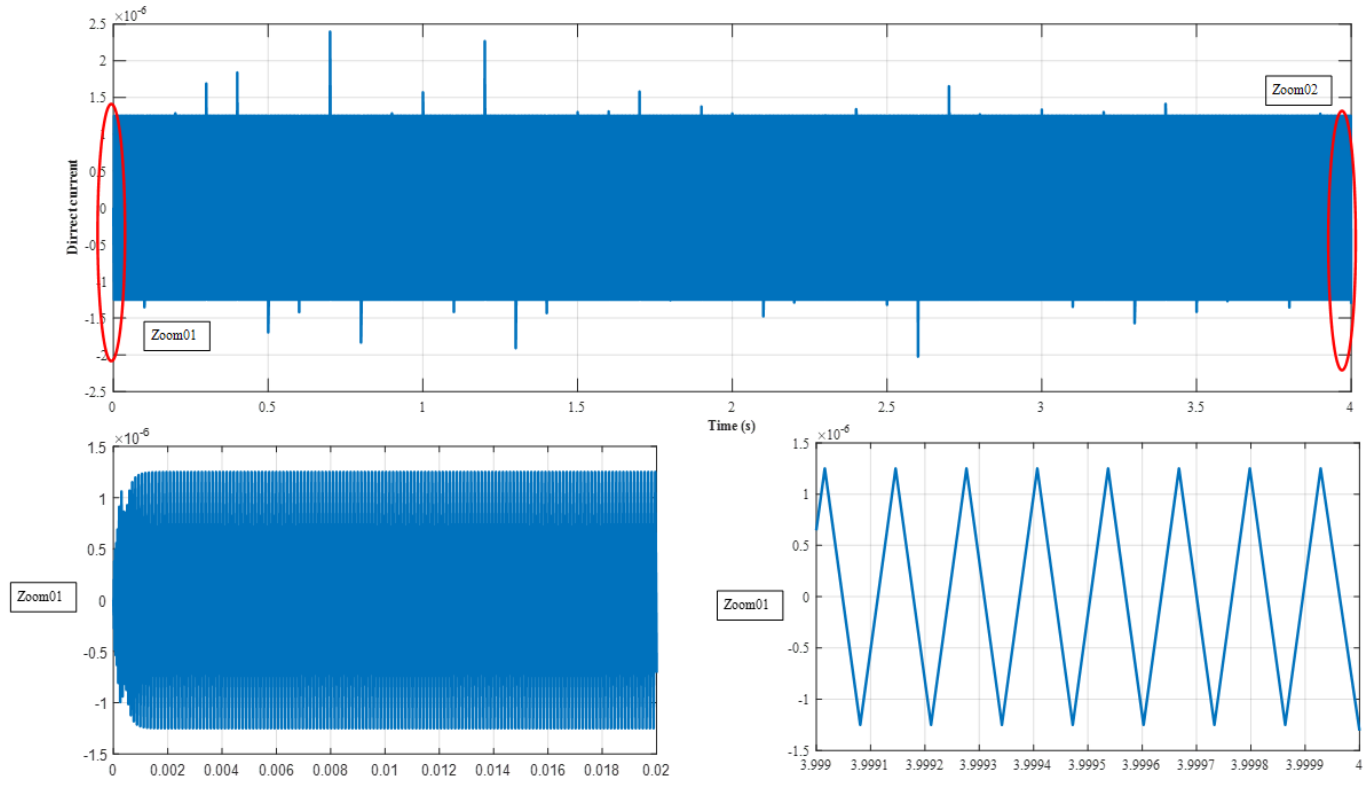

Figure 20. Direct current

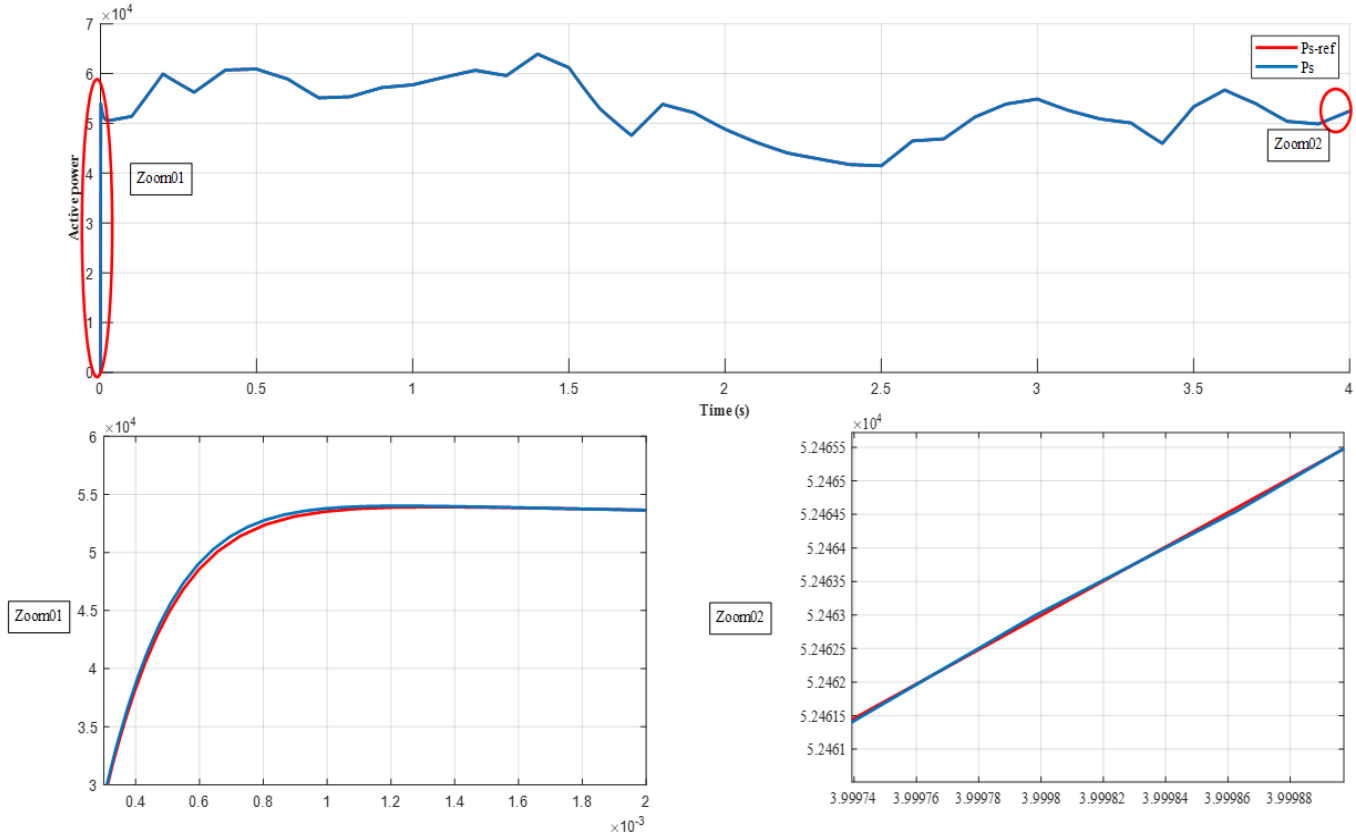

Figure 21. Active power

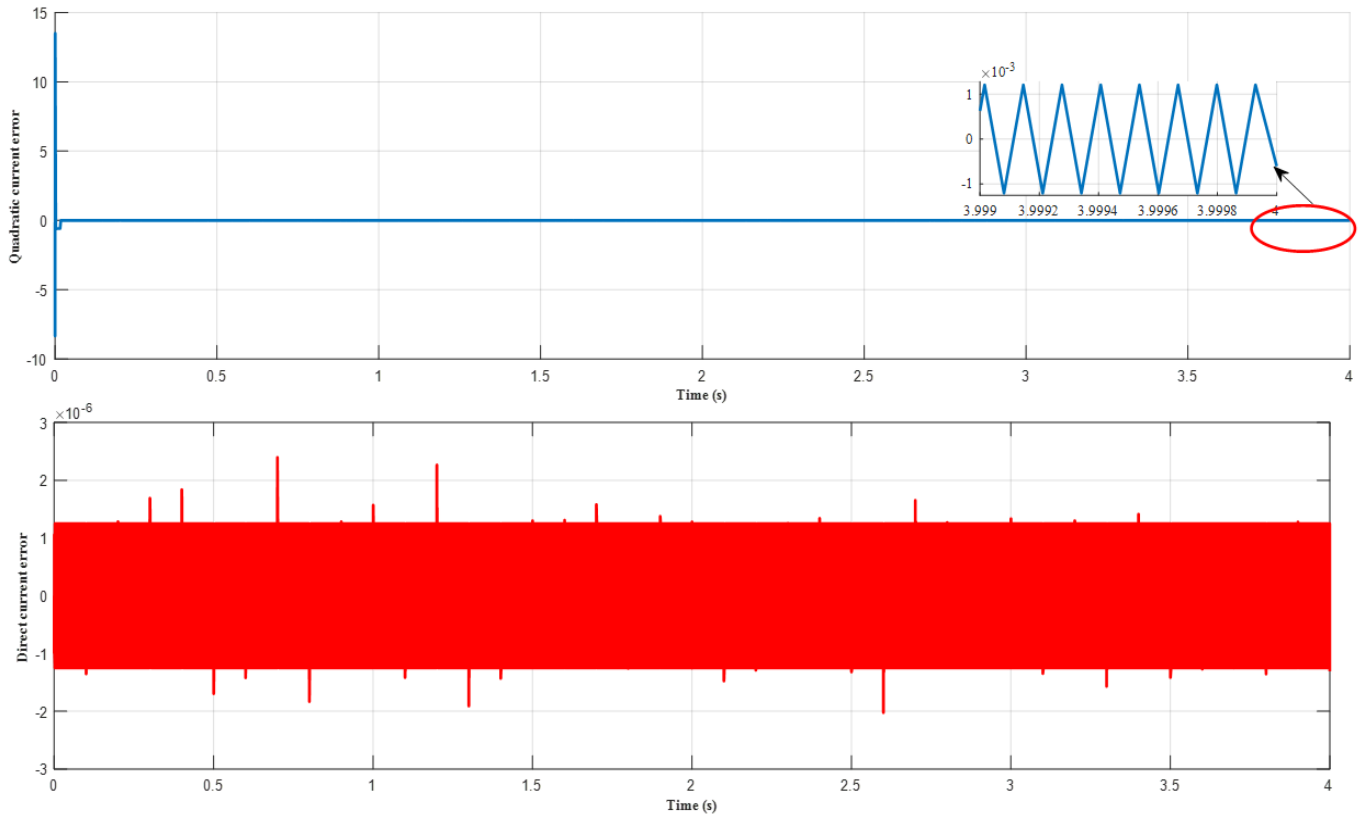

Figure 22. Quadratic and direct current errors

Throughout the rising phase, the current indicates a very slight peak of about 1288.12 A, which is equivalent to an absolute overshoot of about 1.03 A, or about 0.08% of the final figure. With a settling time of 1.4×10^{-3} s and a steady-state inaccuracy of just 6.04×10^{-2}, the divergence from the reference is almost insignificant. The efficiency of the hybrid

PSO–ISMC controller is further demonstrated by a zoomed-in view, which shows very little chattering around the reference and just slight oscillations. Figure 20 depicts the direct current response achieved with the proposed approach, showing minimal chattering around the zero reference and occasional peaks, which reflect the high precision of the control strategy.

A very small chattering around the reference power is observed using the hybrid GWO–ISMC approach, as illustrated in Figure 21. Figure 22 illustrates the tracking errors of the quadratic current (in blue) and the direct current (in red) with respect to their reference values.

The quadratic current error exhibits very small oscillations around zero, with an amplitude of approximately 10^{-3}, while the direct current error remains extremely low, fluctuating near zero with an amplitude of about 1.2×10^{-6}, along with the presence of a few transient peaks. These results underscore the high precision and effectiveness of the proposed GWO–ISMC control strategy in ensuring accurate current regulation.

5.5 Simulation 05: Hybrid Particle Swarm Optimization–Grey Wolf Optimizer

Table 4 presents the results obtained for the different configurations of the hybrid PSO–GWO algorithm, showing the influence of fitness functions and weightings on computational time, and tracking error.

Table 4. The obtained results with hybrid Particle Swarm Optimization–Grey Wolf Optimizer (PSO–GWO) algorithm

Fitness Function	Weights	Time	e_d	e_q
Absolute Integral Error (AIE)	$w_1 = 1$ $w_2 = 1$	$2.91e^{+3}$	2.44×10^{-7}	-8.55×10^{-3}
	$w_1 = 0.5$ $w_2 = 0.5$	$2.22e^{+3}$	1.88×10^{-7}	-1.15×10^{-2}
	$w_1 = 0.25$ $w_2 = 0.75$	$2.86e^{+3}$	-5.20×10^{-8}	1.94×10^{-3}
	$w_1 = 0.75$ $w_2 = 0.25$	$2.84e^{+3}$	3.31×10^{-7}	3.43×10^{-2}
Squared Integral Error (SIE)	$w_1 = 1$ $w_2 = 1$	$4.22e^{+3}$	4.30×10^{-7}	-2.13×10^{-3}
	$w_1 = 0.5$ $w_2 = 0.5$	$4.22e^{+3}$	-1.73×10^{-7}	-7.58×10^{-4}
	$w_1 = 0.25$ $w_2 = 0.75$	$2.99e^{+3}$	1.52×10^{-7}	-9.28×10^{-4}
	$w_1 = 0.75$ $w_2 = 0.25$	$2.68e^{+3}$	-5.21×10^{-7}	2.21×10^{-3}
Temporal Absolute Integral Error (TAIE)	$w_1 = 1$ $w_2 = 1$	$2.33e^{+3}$	-4.11×10^{-7}	3.51×10^{-3}
	$w_1 = 0.5$ $w_2 = 0.5$	$2.22e^{+3}$	-3.01×10^{-7}	3.19×10^{-3}
	$w_1 = 0.25$ $w_2 = 0.75$	$4.15e^{+3}$	1.06×10^{-6}	-4.50×10^{-4}
	$w_1 = 0.75$ $w_2 = 0.25$	$2.29e^{+3}$	-4.36×10^{-7}	-7.09×10^{-4}
Temporal Squared Integral Error (TSIE)	$w_1 = 1$ $w_2 = 1$	$2.35e^{+3}$	8.49×10^{-7}	1.91×10^{-3}
	$w_1 = 0.5$ $w_2 = 0.5$	$2.33e^{+3}$	5.324×10^{-7}	3.27×10^{-3}
	$w_1 = 0.25$ $w_2 = 0.75$	$2.27e^{+3}$	1.20×10^{-6}	-2.30×10^{-3}
	$w_1 = 0.75$ $w_2 = 0.25$	$2.21e^{+3}$	1.06×10^{-6}	-4.50×10^{-4}

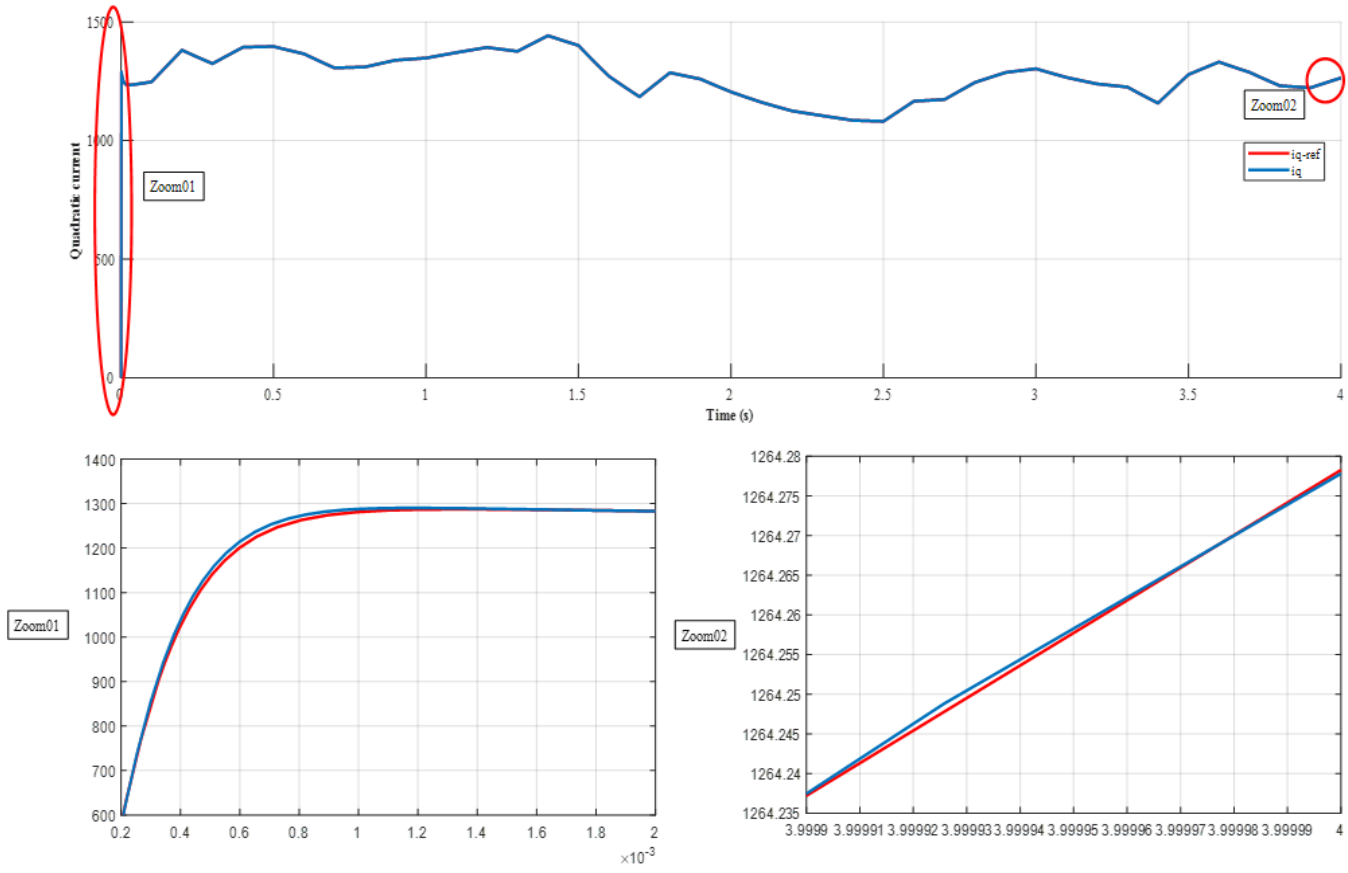

Figure 23. Quadratic current

The hybrid PSO–GWO algorithm effectively combines the fast convergence of GWO with the robust search capabilities of PSO, resulting in a well-balanced and efficient optimization strategy. Among the different configurations tested, those based on the TAIE fitness function with $w_1 = 0.25$ and $w_2 = 0.75$, as well as TSIE with $w_1 = 0.75$ and $w_2 = 0.25$, offer the most balanced performance, achieving good precision while maintaining acceptable computation times. Notably, the configuration using the TSIE fitness function stands out as the fastest among all hybrid cases.

Figures 23-26 illustrate the system's performance under the optimal configuration, as determined through the optimization process. Using the hybrid PSO–GWO–ISMC approach, only minimal chattering is observed around the reference value of the quadratic current. The steady-state error is extremely low at 4.50×10^{-4}, with a slight peak of approximately 1289.59 A, corresponding to an absolute overshoot of 2.5 A (≈ 0.19%) and a settling time of 1.4×10^{-3} s, as shown in Figure 23. A zoomed-in view further confirms the limited chattering and minor oscillations around the reference, highlighting the controller's effectiveness in both transient and steady-state regimes.

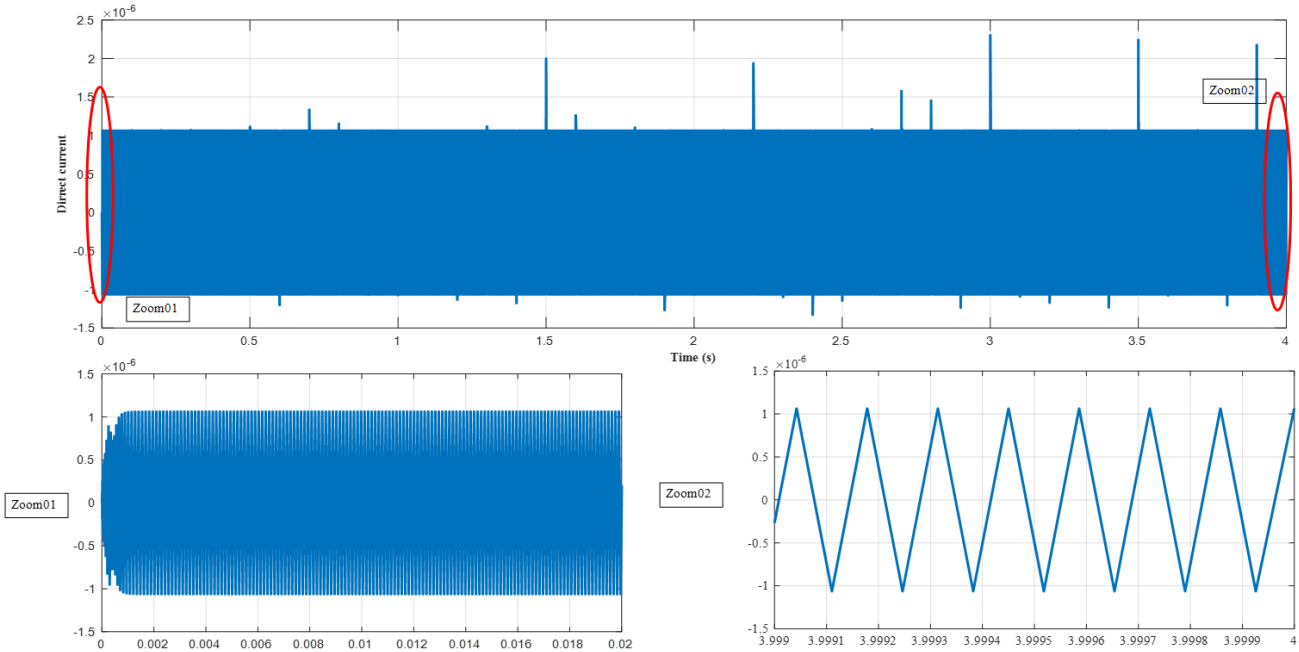

Figure 24. Direct current

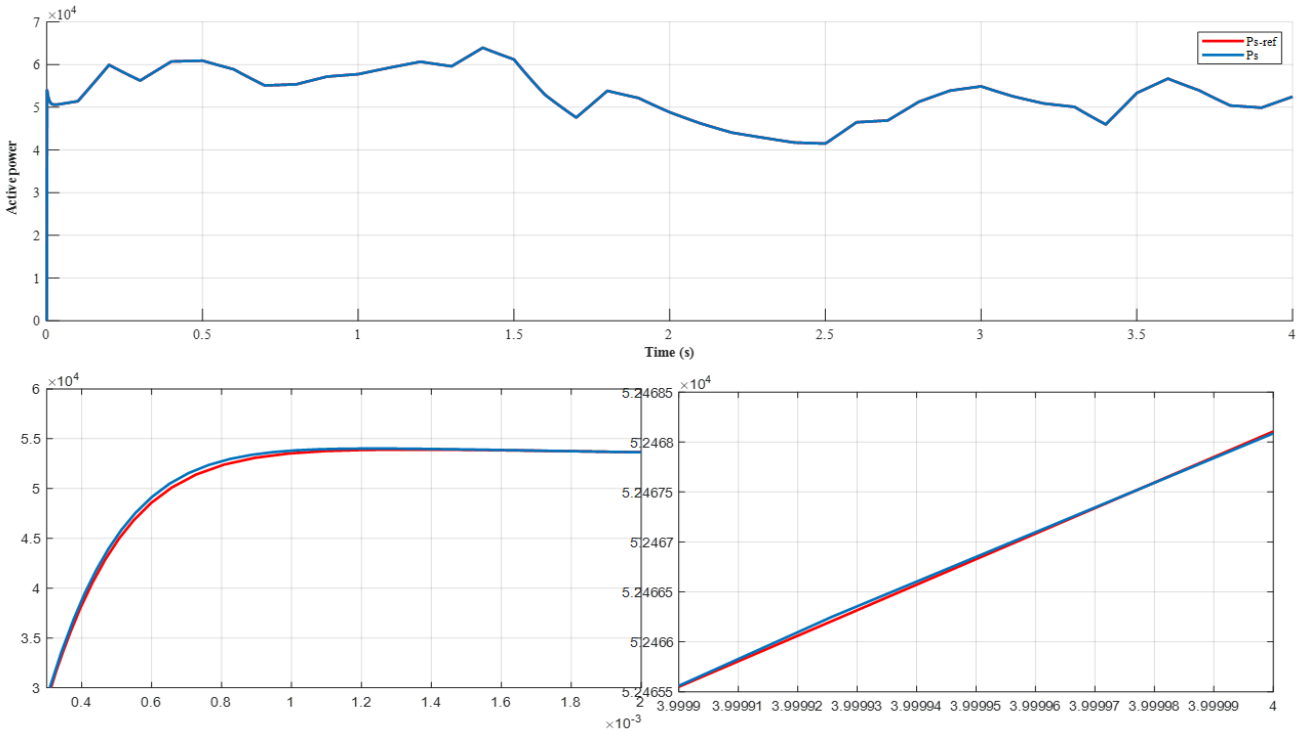

Figure 25. Active power

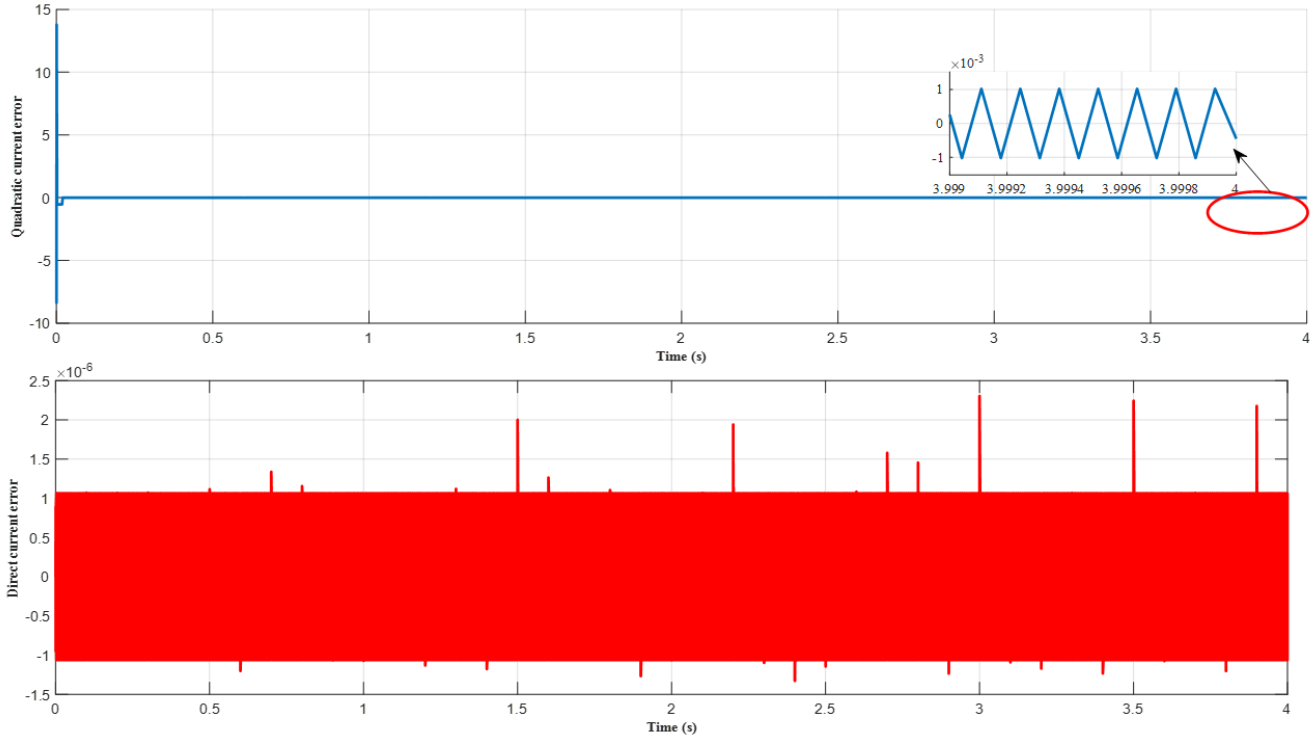

Figure 26. Quadratic and direct current errors

As shown in Figure 24, the proposed control scheme yields a direct current response with negligible chattering around the zero reference and occasional small peaks, underscoring its precise regulation capability of the proposed approach. Figure 25 demonstrates that the hybrid PSO–GWO–ISMC approach achieves an exceptionally smooth power response around the reference value. Figure 26 illustrates the error curves for the quadratic current (in blue) (the deviation from its reference) and the direct current (in red) (relative to its zero reference) using the PSOGWO–ISMC approach.

The results confirm the method's effectiveness in substantially reducing chattering amplitude for both error signals. The obtained results demonstrate that advanced metaheuristic optimization, particularly the GWO and various PSO-based strategies, significantly enhance the performance of ISMC in WECSs. Extensive simulations under variable wind conditions confirm that tuning ISMC gains through these algorithms reduces steady-state error, improves dynamic response, and effectively mitigates chattering, thereby increasing both reliability and efficiency.

A key finding is the decisive influence of the fitness function and its weighting. The TSIE, with an asymmetric weighting of $w_1 = 0.25$ and $w_2 = 0.75$, consistently outperforms other criteria, achieving an average computation time reduction of 42% while maintaining residual errors below 10^{-6} for i_d and 10^{-3} for i_q across GWO, PSO-*fmincon*, and PSO–GWO methods. This asymmetric distribution proves critical for penalizing late-stage deviations of the quadratic current i_q.

Overall, the integration of the hybrid PSO–GWO approach, guided by the TSIE fitness function with $w_1 = 0.25$ and $w_2 = 0.75$, provides a robust and well-balanced control solution.

6. CONCLUSIONS

In this study, we first developed a comprehensive model of a WECS driven by a PMSG and designed an ISMC–FOC architecture to regulate the quadratic and direct currents. To achieve optimal controller performance, four metaheuristic algorithms the PSO, PSO-*fmincon*, GWO, and the hybrid PSO–GWO were employed, and the tuning problem was formulated as a multi-objective optimization task. Using several scalarization strategies, these multi-objective criteria were converted into single-objective fitness functions, enabling a fair and systematic comparison.

A detailed performance analysis showed that the choice of the optimization criterion plays a decisive role in the controller's behavior. Among the four tested objective functions (AIE, SIE, TAIE, TSIE), the TSIE formulation with asymmetric weighting ($w_1 = 0.25$, $w_2 = 0.75$) consistently delivered the most favorable results by strongly penalizing late-stage current-tracking deviations. The algorithmic comparison revealed that GWO provided the fastest convergence, PSO ensured accurate but slower performance, and PSO-*fmincon* offered highly precise local refinement at a higher computational cost. The hybrid PSO–GWO approach achieved the best global trade-off, combining rapid convergence, low chattering levels, and high tracking accuracy. Simulations confirmed very low dq-current errors (10^{-6}, 10^{-7}), significant chattering suppression, accurate active-power tracking, and an overall improvement in transient dynamics. These findings directly address the reviewer's comment by demonstrating, through quantitative evidence, why the hybrid PSO–GWO guided by the TSIE criterion represents the most robust and balanced optimization strategy for ISMC tuning.

Future work will focus on experimental validation of the optimized controller, either on a physical WECS prototype or through a Hardware-in-the-Loop platform, in order to assess its behavior under realistic disturbances and further refine its real-time applicability.

ACKNOWLEDGMENT

The authors wish to extend their sincere gratitude to the Deanship of Scientific Research at the Islamic University of Madinah for the support provided to the Post Publishing Program.

REFERENCES

[1] Bouguettah, I., Messadi, M., Kemih, K., Azar, A.T., Mahlous, A.R. (2024). Adaptive passive fault tolerant control of DFIG-based wind turbine using a self-tuning fractional integral sliding mode control. Frontiers in Energy Research, 12: 1429877. https://doi.org/10.3389/fenrg.2024.1429877

[2] Rinnovabili. (2024). Global electricity consumption hits record high in 2024: Climate, AI, and EVs drive the surge. Rinnovabili. https://www.rinnovabili.net/business/utilities/global-electricity-consumption-2024-record-surge-driven-by-ai-and-evs/.

[3] Ambrose, J. (2025). EVs and datacentres driving new global 'age of electricity', says watchdog. The Guardian. https://www.theguardian.com/business/2025/feb/14/electric-cars-datacentres-new-global-age-of-electricity.

[4] WWEA. (2024). WWEA Annual Report 2023. https://wwindea.org/AnnualReport2023.

[5] Yaramasu, V., Dekka, A., Durán, M.J., Kouro, S., Wu, B. (2017). PMSG-based wind energy conversion systems: Survey on power converters and controls. IET Electric Power Applications, 11(6): 956-968. https://doi.org/10.1049/iet-epa.2016.0799

[6] Matayoshi, H., Howlader, A.M., Datta, M., Senjyu, T. (2018). Control strategy of PMSG based wind energy conversion system under strong wind conditions. Energy for Sustainable Development, 45: 211-218. https://doi.org/10.1016/j.esd.2018.07.001

[7] Arabi, M., Chetioui, L., Zennir, Y., Bounezour, H., Garcia, J.A.S. (2025). Optimal power generation control of wind turbine by using different meta-Heuristic algorithms. Algerian Journal of Signals and Systems, 10(1): 1-6. https://doi.org/10.51485/ajss.v10i1.256

[8] Yachir, A., Merabet Boulouiha, H., Belabbes, A., Khodja, M., Bouddou, R. (2024). Control of a grid-connected PMSG-based wind energy system with a back-to-back converter using a hybrid fuzzy sliding mode control. Przegląd Elektrotechniczny. https://doi.org/10.15199/48.2024.09.15

[9] Bellarbi, S., Koussa, D.S., Djoudi, A. (2018). Sliding mode control for PMSG-based wind power system. Journal of Physics: Conference Series, 1081: 012012. https://doi.org/10.1088/1742-6596/1081/1/012012

[10] Azar, A.T., Serrano, F.E. (2015). Stabilization and control of mechanical systems with backlash. In Handbook of Research on Advanced Intelligent Control Engineering and Automation, pp. 1-60. https://doi.org/10.4018/978-1-4666-7248-2.ch001

[11] Kalel, D., Singh, R.R. (2024). IoT integrated adaptive fault tolerant control for induction motor based critical load applications. Engineering Science and Technology, an International Journal, 51: 101585. https://doi.org/10.1016/j.jestch.2023.101585

[12] Majout, B., Bossoufi, B., Bouderbala, M., Masud, M., Al-Amri, J.F., Taoussi, M., El Mahfoud, M., Motahhir, S., Karim, M. (2022). Improvement of PMSG-based wind energy conversion system using developed sliding mode control. Energies, 15(5): 1625. https://doi.org/10.3390/en15051625

[13] Zine Laabidine, N., Bossoufi, B., El Kafazi, I., El Bekkali, C., El Ouanjli, N. (2023). Robust adaptive super twisting algorithm sliding mode control of a wind system based on the PMSG generator. Sustainability, 15(14): 10792. https://doi.org/10.3390/su151410792

[14] Douara, B.O., Kouzou, A., Hafaifa, A., Rodriguez, J., Abdelrahem, M. (2025). An enhanced second-order terminal sliding mode control based on the super-twisting algorithm applied to a five-phase permanent magnet synchronous generator for a grid-connected wind energy conversion system. Energies, 18(2): 355. https://doi.org/10.3390/en18020355

[15] Belabbes, A., Laidani, A., Yachir, A., Bouzid, A.E.M., Bouddou, R., Litim, O.A. (2024). Advanced control of PMSG-based wind energy conversion system using model predictive and sliding mode control. Przegląd Elektrotechniczny, 2024(2): 10-16. https://doi.org/10.15199/48.2024.02.02

[16] Messadi, M., Mellit, A., Kemih, K., Ghanes, M. (2015). Predictive control of a chaotic permanent magnet synchronous generator in a wind turbine system. Chinese Physics B, 24(1): 1010502. https://doi.org/10.1088/1674-1056/24/1/010502

[17] Aboulem, S., Boufounas, E.M., Boumhidi, I. (2019). Intelligent proportional-integral sliding mode control of wind turbine systems based particle swarm optimization. International Journal of Automation and Control, 13(3): 347-373. https://doi.org/10.1504/IJAAC.2019.098585

[18] Ben Ali, R., Schulte, H., Mami, A. (2017). Modeling and simulation of a small wind turbine system based on PMSG generator. In 2017 Evolving and Adaptive Intelligent Systems (EAIS), Ljubljana, Slovenia, pp. 1-6. https://doi.org/10.1109/EAIS.2017.7954833

[19] Jisha, L.K., Thomas, A.A.P. (2013). A comparative study on scalar and vector control of Induction motor drives. In 2013 International conference on Circuits, Controls and Communications (CCUBE), Bengaluru, India, pp. 1-5. https://doi.org/10.1109/CCUBE.2013.6718554

[20] Rachev, E., Petrov, V., Vacheva, G. (2025). Comparing V/F and vector control for induction motors in steady-state mode of operation. In 2025 19th Conference on Electrical Machines, Drives and Power Systems (ELMA), Sofia, Bulgaria, pp. 1-5. https://doi.org/10.1109/ELMA65795.2025.11083485

[21] Thayumanavan, P., Muthu, R., Sankararaman, J. (2014). Sensor-less field oriented control of wind turbine driven permanent magnet synchronous generator using flux linkage and back EMF estimation methods. Research Journal of Applied Sciences, Engineering and Technology, 7(20): 4303-4312. https://doi.org/10.19026/rjaset.7.802

[22] Jain, B., Jain, S., Nema, R.K. (2015). Control strategies of grid interfaced wind energy conversion system: An overview. Renewable and Sustainable Energy Reviews, 47: 983-996. https://doi.org/10.1016/j.rser.2015.03.063

[23] Shehata, E.G. (2017). A comparative study of current control schemes for a direct-driven PMSG wind energy generation system. Electric Power Systems Research, 143: 197-205. https://doi.org/10.1016/j.epsr.2016.10.039

[24] Lotfi, C., Youcef, Z., Marwa, A., Schulte, H., El-Arkam, M., Riad, B. (2023). Optimization of a speed controller of a WECS with metaheuristic algorithms. Engineering Proceedings, 29(1): 7. https://doi.org/10.3390/engproc2023029007

[25] Lotfi, C., Youcef, Z., Marwa, A., Schulte, H., Riad, B., El-Arkam, M. (2023). Optimization of a speed controller of a DFIM with metaheuristic algorithms. Engineering Proceedings, 29(1): 13. https://doi.org/10.3390/engproc2023029013

[26] Mirjalili, S., Mirjalili, S.M., Lewis, A. (2014). Grey wolf optimizer. Advances in Engineering Software, 69: 46-61. https://doi.org/10.1016/j.advengsoft.2013.12.007

[27] Ouguissi, H., Saadi, S., Errahmane, H., Benmessaoud, A., Rabehi, A. (2025). Chua Chaotic system parameters estimation using PSO algorithm to increase its dynamics. Islamic University Journal of Applied Sciences, VII(I): 138-148. https://doi.org/10.63070/jesc.2025.009

[28] Kamboj, V.K. (2016). A novel hybrid PSO–GWO approach for unit commitment problem. Neural Computing and Applications, 27: 1643-1655. https://doi.org/10.1007/s00521-015-1962-4

[29] Arabi, M., Zennir, Y., Bourourou, F. (2023). Wind turbine mechanical speed regulation reliability of artificial intelligent PSO-FLC control. In 2023 International Conference on Electrical Engineering and Advanced Technology (ICEEAT), Batna, Algeria, pp. 1-5. https://doi.org/10.1109/ICEEAT60471.2023.10426248

[30] Utkin, V., Shi, J.X. (1996). Integral sliding mode in systems operating under uncertainty conditions. In Proceedings of 35th IEEE Conference on Decision and Control, Kobe, Japan, pp. 4591-4596. https://doi.org/10.1109/cdc.1996.577594

[31] El Mourabit, Y., Derouich, A., El Ghzizal, A., Bouchnaif, J., El Ouanjli, N., Zamzoum, O., Mezioui, K., Bossoufi, B. (2019). Implementation and validation of backstepping control for PMSG wind turbine using dSPACE controller board. Energy Reports, 5: 807-821. https://doi.org/10.1016/j.egyr.2019.06.015

[32] Merzoug, M.S., Benalla, H., Louze, L. (2012). Sliding mode control (SMC) of permanent magnet synchronous generators (PMSG). Energy Procedia, 18: 43-52. https://doi.org/10.1016/j.egypro.2012.05.016

[33] Sellami, M., Dourari, A.L., Bagua, H. (2025). Photovoltaic cells fed a dual open-end winding induction motor driven by fuzzy field-oriented control. Islamic University Journal of Applied Sciences, VII(I): 178-191. https://doi.org/10.63070/jesc.2025.011

[34] Lian, J., Zhao, J., Dimirovski, G.M. (2010). Integral sliding mode control for a class of uncertain switched nonlinear systems. European Journal of Control, 16(1): 16-22. https://doi.org/10.3166/ejc.16.16-22

[35] Hamdaoui, M. (2010). Optimisation multicriteres de l'efficacite propulsive de mini-drones biomimetiques a ailes battantes par algorithmes evolutionnaires. Sciences de l'ingénieur [physics]. Université Pierre et Marie Curie - Paris VI. https://hal.science/tel-00550437/.

[36] Corradini, M.L., Ippoliti, G., Orlando, G. (2013). Fully sensorless robust control of variable-speed wind turbines for efficiency maximization. Automatica, 49(10): 3023-3031. https://doi.org/10.1016/j.automatica.2013.07.028

[37] Muro, C., Escobedo, R., Spector, L., Coppinger, R.P. (2011). Wolf-pack (*Canis lupus*) hunting strategies emerge from simple rules in computational simulations. Behavioural Processes, 88(3): 192-197. https://doi.org/10.1016/j.beproc.2011.09.006

[38] Al-Butti, O.S., Altinoz, O.T. (2023). Comparison between PSO-based and *fmincon*-based approaches of optimal power flow for a standard IEEE-30 bus system. In Proceedings of the 2022 International Symposium on Energy Management and Sustainability. ISEMAS 2022. Springer Proceedings in Energy, pp. 209-219. https://doi.org/10.1007/978-3-031-30171-1_23

[39] Shaheen, M.A.M., Hasanien, H.M., Alkuhayli, A. (2021). A novel hybrid GWO-PSO optimization technique for optimal reactive power dispatch problem solution. Ain Shams Engineering Journal, 12(1): 621-630. https://doi.org/10.1016/j.asej.2020.07.011